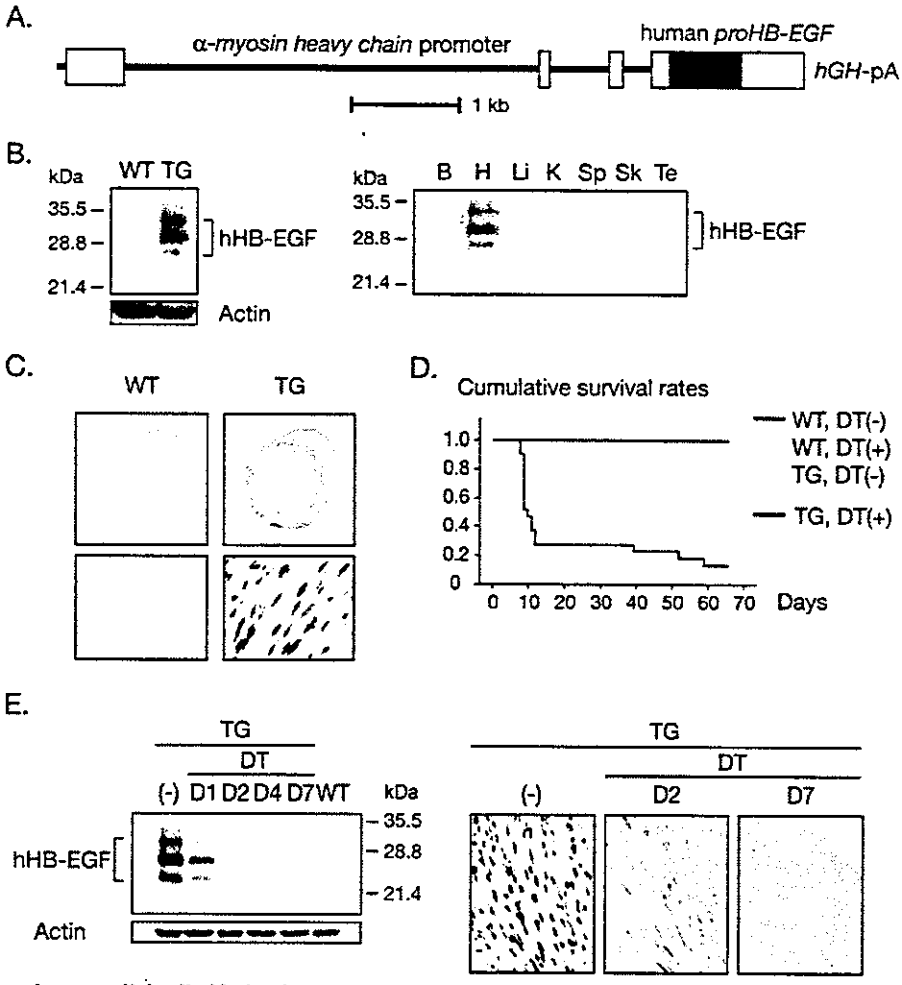

FIG. 1. **DT-induced myocardial cell ablation in transgenic mice expressing human *pro-HB-EGF*.** *A*, schematic representation of the transgene containing α-myosin heavy chain (*αMHC*) promoter, human *pro-HB-EGF* cDNA, and human growth hormone (*GH*) polyadenylation signal (*pA*). *B*, Western blot analysis using an antibody specific for human pro-HB-EGF revealed transgene expression in TG hearts (*left*). Expression of human pro-HB-EGF in TG was observed specifically in the hearts (*right*). *B*, brain; *H*, heart; *Li*, liver; *K*, kidney; *Sp*, spleen; *Sk*, skeletal muscle; *Te*, testis. *C*, *in situ* hybridization analysis using a riboprobe specific for human *pro-HB-EGF*. Transgene was expressed in a mosaic pattern, and cardiomyocytes expressing the transgene were 17.3 ± 6.0% of the total cardiomyocytes within TG hearts. *D*, Kaplan-Meier survival curves of control mice (WT treated with mock or DT and TG treated with mock, $n = 21$, respectively) and TG ($n = 21$) treated with intramuscular injection of DT. *E*, complete ablation of transgene-expressing cardiomyocytes following DT injection revealed by immunoblot (*left*) and *in situ* hybridization analysis. Expression of pro-HB-EGF was remarkably diminished on day 2 (*D2*) and was completely undetected on day 7 (*D7*).

sections of TG hearts on 14 days after DT injection revealed a 1.9-fold increase in cross-sectional areas of cardiomyocytes (Fig. 3*C*), indicating that the cardiomyocytes, which did not express the transgene and survived DT administration, underwent hypertrophic cell growth.

Alterations of Gene Expression in TG Presenting DT-induced Heart Failure—To characterize the molecular basis of heart failure caused by DT-induced myocardial cell ablation, we examined expression levels of several molecular markers. Expression of *BNP* was up-regulated 1 day after DT injection, and persistently elevated thereafter (Fig. 4). Increased expression of skeletal α-actin and decreased expression of *SERCA2* were evident 4 days after DT injection (Fig. 4). Up-regulation of natriuretic peptide genes and fetal cardiac genes including skeletal α-actin is one of the characteristic cellular responses observed during cardiac hypertrophy (32, 33). Especially, ventricular expression of *BNP* is induced promptly in response to volume expansion and pressure overload, and plasma BNP concentrations have proven to be valuable for diagnostic and prognostic assessment in patients with heart failure (34). In addition, down-regulation of *SERCA2* has been reported to be a sensitive marker for heart failure (35). Therefore, these patterns of cardiac gene expression indicated that DT-induced myocardial cell ablation burdened hemodynamic overload and progressed overt heart failure concomitantly with cardiac hypertrophy.

Consistent with the histological finding of infiltration by macrophages, an increase in expression of *MCP-1* was observed 1 day after DT injection, and expression levels of *MCP-1* were further increased until 4 days and declined on 7 days (Fig. 4). The expression levels of *TNF-α*, encoding an inflammatory cytokine produced by macrophages, changed in parallel with that of *MCP-1* (Fig. 4). Insomuch as symptomatic heart failure was evident 7 days after DT injection, stressed myocardium could be another source of *TNF-α* production at this period. Following up-regulation of inflammatory markers, expression levels of the collagen genes (*Col1a2* and *Col3a1*) were increased at 4 days after DT injection (Fig. 4). These temporal profiles of

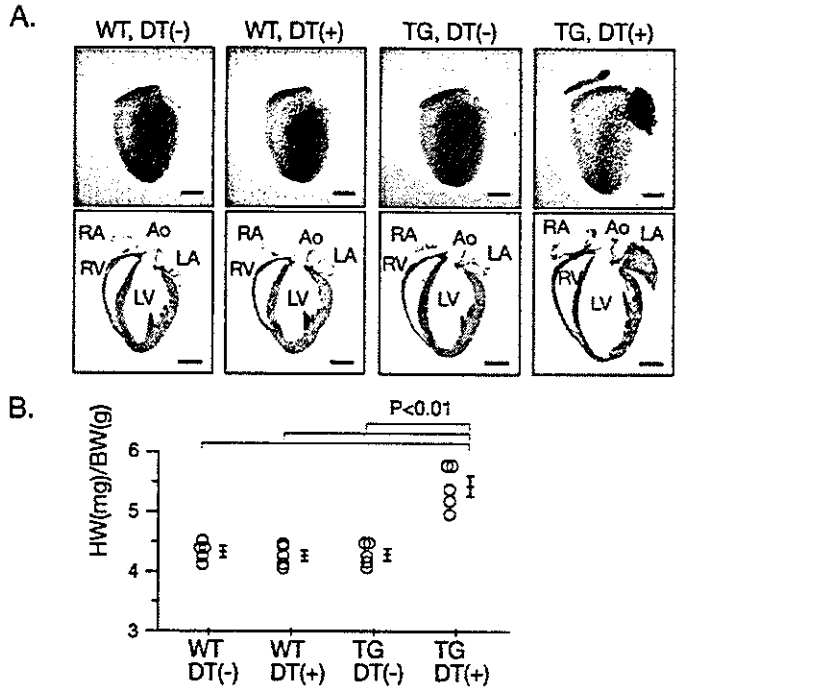

D.

	WT, DT(-)	WT, DT(+)	TG, DT(-)	TG, DT(+)
Number	10	10	10	10
Age (weeks)	10.7±0.4	10.6±0.5	11.5±0.3	10.9±0.3
BW(g)	24.0±1.7	24.1±1.2	24.8±0.4	24.3±1.3
HR (beats/min.)	261.0±15.9	258.9±18.8	256.3±18.4	252.3±18.0
LVDd (mm)	3.69±0.14	3.71±0.17	3.75±0.23	4.69±0.71
LVDs (mm)	2.05±0.13	2.11±0.20	2.08±0.27	3.81±0.46
FS (%)	44.2±4.7	43.2±4.9	47.4±3.5	19.4±3.0
IVSth (mm)	0.65±0.03	0.65±0.03	0.66±0.02	0.45±0.03
LVPWth (mm)	0.65±0.03	0.66±0.02	0.66±0.02	0.39±0.03

FIG. 2. **DT-induced cardiomyocyte loss caused heart failure in mice.** *A*, gross morphology of whole hearts (*upper rows*) and longitudinal sections (*lower rows*) of WT and TG 7 days after DT or mock injection. *Ao*, aorta; *LA*, left atrium; *LV*, left ventricle; *RA*, right atrium; *RV*, right ventricle. *Bar*, 2 mm. *B*, increase in heart to body weight ratios observed in TG 7 days after DT injection. *C*, representative M-mode echocardiograms. *IVS*, interventricular septum; *LVPW*, left ventricular posterior wall. *D*, echocardiographic measurements. *BW*, body weight; *FS*, fractional shortening; *HR*, heart rate; *IVSth*, interventricular thickness in end-diastole; *LVDd*, left ventricular diameter in end-diastole; *LVDs*, left ventricular diameter in end-systole; *LVPWth*, left ventricular posterior wall thickness in end-diastole.

gene expressions suggest that mobilization of macrophages are induced by up-regulated MCP-1 after the myocardial cell ablation, leading to cardiac fibrosis by enhanced production of inflammatory cytokines, and that inflammatory cytokines and cardiac remodeling might promote left ventricular dysfunction evoked by myocardial cell loss.

Myocardial Cell Death Induced by DT Is Not Primarily because of Apoptosis—To investigate the mechanisms of myocardial cell death in DT-treated TG hearts, we first performed a TUNEL assay. In the hearts of DT-treated TG, we could not detect any TUNEL-positive cardiomyocytes or inflammatory cells, whereas a marked increase in TUNEL-positive cells was detected in the spleen of mice treated with intraperitoneal administration of lipopolysaccharide as positive controls (Fig. 5*A*). Likewise, analysis of genomic DNA by agarose gel provided no evidence of DNA laddering in DT-treated TG hearts (Fig. 5*B*). We further examined activation of caspase 3 (Fig. 5*C*), changes in expression of proapoptotic and antiapoptotic Bcl2 family proteins (Fig. 5*D*), and cytochrome *c* release from mitochondria (Fig. 5*E*), but biochemi-

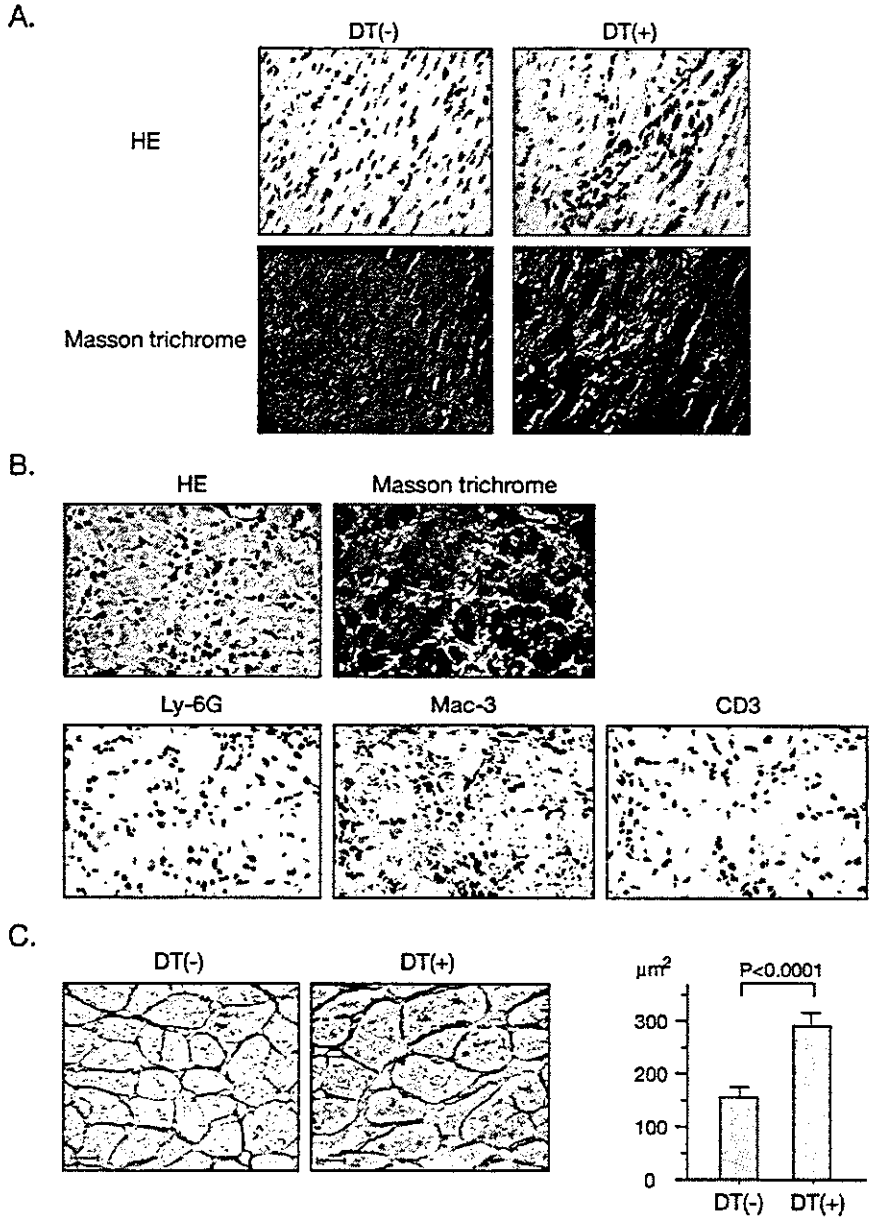

FIG. 3. **Histological analysis of the hearts after DT injection.** *A*, serial sections with hematoxylin-eosin (*HE*) staining revealed cardiomyocyte degeneration and infiltration of inflammatory cells 7 days after DT injection. Masson's trichrome staining showed interstitial fibrosis. *B*, infiltrating inflammatory cells were predominantly macrophages with positive staining for Mac-3 but not for Ly-6G nor CD3. *C*, silver staining of TG hearts 14 days after DT injection revealed an increase in the cross-sectional area of cardiomyocytes, indicating hypertrophic compensation of myocardial cells without transgene expression.

cal changes leading to typical apoptosis were not observed in DT-treated TG hearts.

Autophagy Is the Mechanism of Myocardial Cell Death in DT-induced Failing Hearts—ACD is a regulated process of caspase-independent programmed cell death, in which intracellular components are degradated by lysosomal or proteasomal proteases (21–23). Immunohistochemical analysis revealed positive staining for lysosomal protease cathepsin D, LAMP-1, and ubiquitin in cardiomyocytes of DT-treated TG hearts (Fig. 6*A*). It is notable that cathepsin D showed a diffuse cytosolic distribution, whereas LAMP-1 showed a granular localization. These results suggest an increase in formation of lysosomes and leakage of activated lysosomal enzymes into the cytosol. Recently, it has been reported that, in human failing hearts, ubiquitin accumulation in cardiomyocytes may be associated with up-regulation of ubiquitin-conjugating enzyme E2 (UBC2) and down-regulation of deubiquitinating enzymes such as UFD1 and isopeptidase T (6). However, Western blot analysis revealed that the amounts of the ubiquitin-activating enzyme E1, UBC2, ubiquitin-ligating enzyme E3 (E6-AP), and UFD1 were not unchanged in DT-treated TG hearts when compared with control hearts (Fig. 6*B*).

Electron microscopic analysis revealed abundant cytosolic vacuoles and segmented configuration of nuclei with lumpy con-

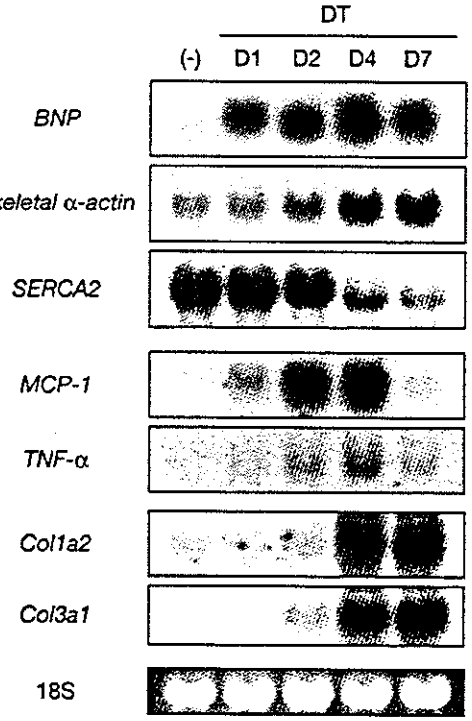

FIG. 4. **Alterations in gene expression after DT injection.** Temporal profiling of gene expression following administration of DT (5 mg/kg). Expression levels of cardiac genes, inflammatory cytokine genes, and collagen genes were examined by Northern blot analysis.

densation of chromatin in degenerated cardiomyocytes in TG hearts 3 days after DT injection (Fig. 7, *A* and *B*). However, nuclear fragmentation and crescent-shaped chromatin condensation at the nuclear periphery typical of apoptosis were not observed. In higher magnifications, cytosolic vacuoles containing lipid droplets with myelin figures and degenerated mitochondria (Fig. 7, *C* and *D*), suggested that these vacuoles are typical autophagosomes. In terminally degenerated cardiomyocytes, lysis of myofibrills and other intracellular organelles were prominent (Fig. 7*E*). These findings suggest that myocardial cell loss in DT-treated TG hearts is primarily because of ACD.

Autophagic degeneration has been implicated in human failing heart failure (3–7). We also found cardiomyocytes undergoing autophagic cell death in a biopsied specimen from a 43-year-old patient suffering from dilated cardiomyopathy. Similar to the electron micrographic findings in degenerated cardiomyocytes in our mouse model of heart failure, myofibrillar degeneration in association with cytosolic vacuoles and lipid droplets were observed in this biopsied specimen (Fig. 7*F*). The vacuoles were autophagosomes containing digested organelles. These findings are illustrative of the previously reported features characteristic of ACD in human heart failure. Therefore, degenerated cardiomyocytes in human dilated cardiomyopathy patients showed ultrastructural alterations similar to those in our mouse model of heart failure.

DISCUSSION

In this study, we generated a novel mouse model of heart failure, where cardiomyocyte loss through ACD is arbitrarily and specifically induced by intramuscular injection of DT. Recent technical progress in genetic manipulation and physiological measurements enabled us to produce several mouse models of heart failure (36). These models have improved our understanding of pathophysiology of heart failure and have been of great help for establishment and evaluation of new therapeutic approaches. Genetically engineered mice, in particular, expanded the list of gene products that are involved in generation or progression of heart failure, but they have specific limitations as animal models. For example, mice homozygous for muscle LIM protein (*MLP*) develop cardiomyopathy and heart failure, but the clinical courses of individual mice are divergent because the penetrance of phenotype is influenced by genetic backgrounds (37). About half of the *MLP*-deficient mice suffer from severe congestive heart failure and die during the second postnatal week, but the rest of the *MLP*-deficient mice survive to adulthood and are viable. Development of cardiomyopathy is also identified in tropomodulin-overexpressing transgenic mice (38). In this model, severe signs of heart failure are observed between 2 and 4 weeks after birth and most symptomatic mice die within a few days. The phenotypes of these model mice are primarily genotype-dependent, but are susceptible to the effects of genetic backgrounds. In addition, a difficulty in morphological and biochemical approach in studying a role of cardiomyocyte death in heart failure arises from the low occurrence of cell death in these models (2). In our mouse model of heart failure, cardiomyocytes expressing the DT receptor are selectively and simultaneously damaged by administration of DT, and this advantageous feature not only makes it possible to induce symptomatic heart failure arbitrarily but also provides insights into the roles of cell death in heart failure.

Our model appears conceptually similar to the one reported in the earlier work (39), in which DT-A expression is regulated by a tetracycline-responsive promoter. In that model, induction of DT-A in the hearts resulted in congestive heart failure as well. However, a leaky induction is occasionally observed in this tetracycline-inducible system, and subtle expression of DT-A might have nonspecific and undesirable effects, insomuch as the toxicity of DT-A is extremely high (17). In our model, the DT receptor, not injurious in the absence of DT, was expressed in the hearts, and myocardial cell ablation was specifically and ideally achieved.

Temporal histological analysis and profiling of gene expression revealed a series of cellular events that finally evoked heart failure (Figs. 3 and 4). Transgene expression was dramatically reduced in a few days after DT injection (Fig. 1*E*), suggesting that cardiomyocyte death occurs during that period. Following cardiomyocyte death, inflammatory cells infiltrated and produced inflammatory cytokines. Around 7 days, hemodynamic deterioration with apparent cardiac remodeling induced symptomatic heart failure. These findings strongly suggest that myocardial cell death causes symptomatic heart failure. In addition, our model allowed quantitative analysis of cardiomyocyte death. *In situ* hybridization analysis revealed that expression of the transgene was scattered diffusely and observed in 17.3 ± 6.0% of cardiomyocytes in TG hearts. Because there was no cardiomyocyte expressing the transgene on day 7 after DT injection, all of the transgene-expressing cells (~17% of cardiomyocytes) might be dead. These results suggest that loss of this population is sufficient to produce symptomatic heart failure, and this estimation is consistent with the notion that a diffuse loss of 10–20% of cardiomyocytes accounts for cardiac failure, whereas equivalent cardiac failure is produced by a segmental loss of 40–50% of cardiomyocytes after coronary artery occlusion (40).

Electron microscopic analysis revealed that, in our mouse model, damaged cardiomyocytes showed abundant cytoplasmic autophagosomes and chromatin condensation with more complex and lumpier shapes than in apoptosis, both of which are characteristic of ACD (Fig. 7). ACD is defined as a regulated pathway of cytoplasmic degradation executed by lysosomal and

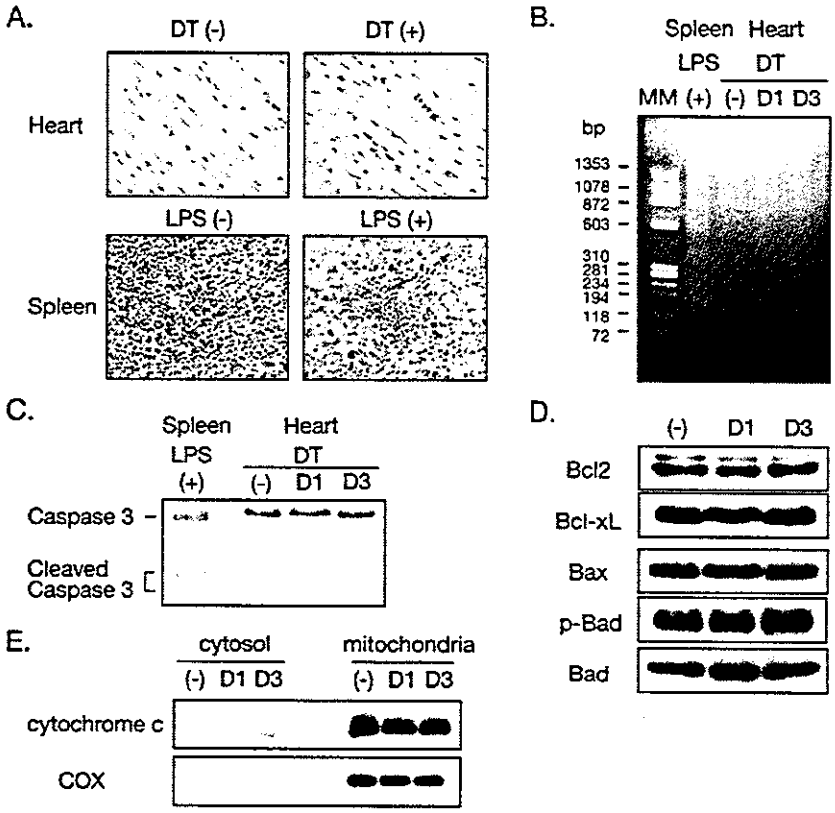

FIG. 5. **DT-induced myocardial cell death is not mediated by apoptosis, but by autophagy.** *A* and *B*, TUNEL method (*A*) and electrophoresis of genomic DNA by agarose gel (*B*) showed no evidence of DNA fragmentation in TG hearts 3 days after DT injection. Spleens from mice with lipopolysaccharide-induced sepsis were used as a positive control. *C–E*, immunoblot analysis showing no evidence of activation of caspase 3 (*C*), changes in expressions of Bcl2 family proteins (*D*) and cytochrome c release from mitochondria (*E*) in DT-treated TG hearts. *COX*, cytochrome c oxidase subunit IV. *D*, day. *LPS*, lipopolysaccharide.

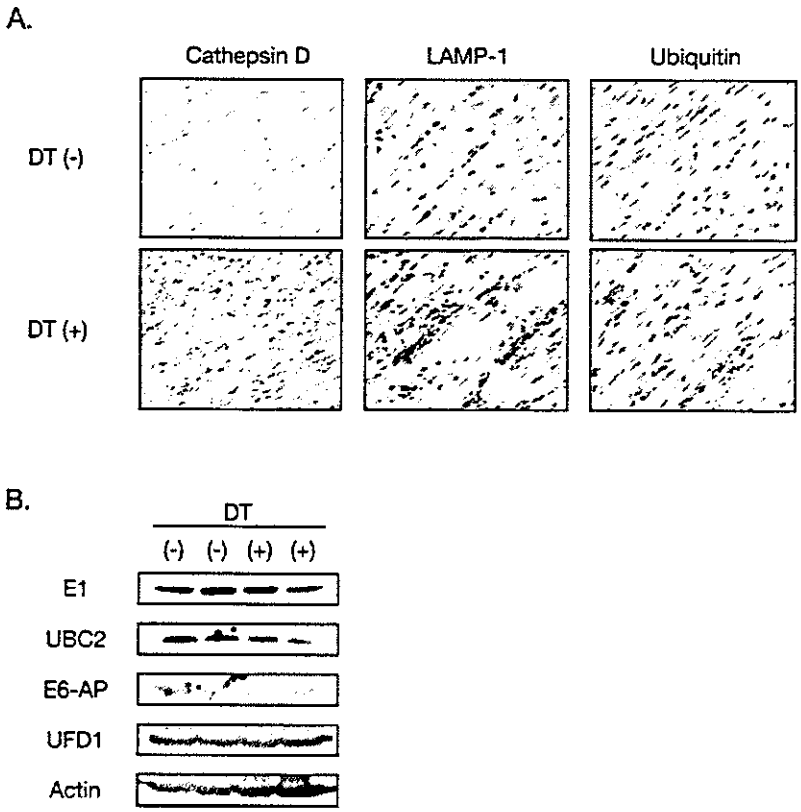

FIG. 6. **DT-induced myocardial cell death is mediated by autophagy.** *A*, immunohistochemistry showing cardiomyocytes were positively stained for cathepsin D, LAMP-1, and ubiquitin in TG hearts 3 days after DT injection. *B*, immunoblot analysis showing unchanged expression levels of the ubiquitin-activating enzyme E1, ubiquitin-conjugating enzyme E2 (*UBC2*), ubiquitin-ligating enzyme E3 (*E6-AP*), and deubiquitinating enzyme UFD1.

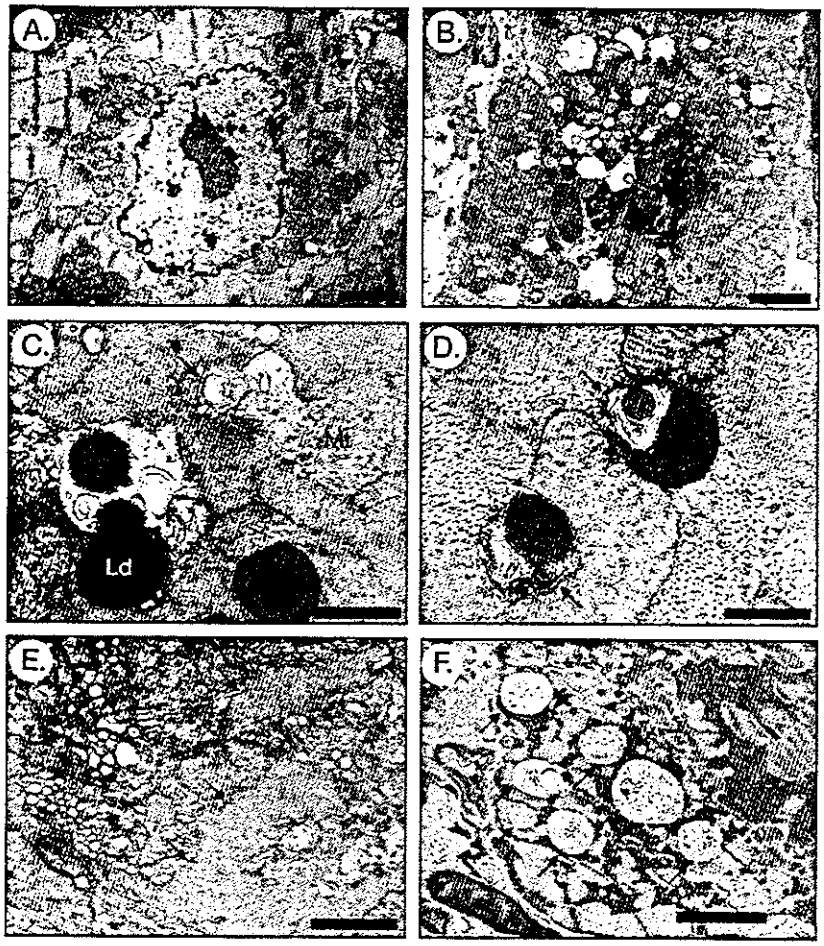

FIG. 7. **Electron microscopic analysis of the hearts after DT injection.** Electron microscopic analysis before (*A*) and after DT injection (*B–E*). In cardiomyocytes of DT-treated TG hearts, nuclear morphological changes associated with lumpy chromatin condensation were observed (*arrow* in *B*). Abundant vacuoles of various sizes in the cytoplasm (*B*) were typical autophagosomes containing degenerating lipid droplets and mitochondria (*C* and *D*). *Arrows* (in *C* and *D*) indicate myelin figures. Myofibrillar lysis (*arrows*) was observed in cardiomyocytes undergoing autophagic cell death (*E*). Electron microscopic analysis of biopsied myocardium from a patient with dilated cardiomyopathy (*F*) revealed cardiomyocytes containing many autophagosomes with degenerating mitochondria (*arrows*). *Ld*, lipid droplet; *Mt*, mitochondria. *Bars*, 2 μm (*A* and *B*), 1 μm (*C* and *E*), 0.5 μm (*D*), and 5 μm (*F*).

proteasomal proteases (21–23, 41). Consistently, elevated expressions of cathepsin D and ubiquitin were recognized in DT-treated TG cardiomyocytes (Fig. 6*A*). In contrast, biochemical signals inducing apoptosis were not activated. ACD often occurs in large, cytoplasmic-rich, and post-mitotic cells, and has been implicated in several human diseases (19, 21–23, 41). For example, ACD is associated with neurodegenerative diseases such as Parkinson's disease (42), Huntington's disease (43), and Alzheimer's disease (44). Degenerated cardiomyocytes displaying morphological features characteristic of ACD have recently been reported to exist in the failing hearts of patients with dilated cardiomyopathy, valvular heart diseases, congenital heart diseases, and hypertensive heart diseases (Fig. 7*F*) (3–7). A recent paper demonstrated that cardiomyocyte apoptosis of rare occurrence comparable with that observed in human failing hearts were sufficient to cause lethal cardiomyopathy in transgenic mice with a ligand-induced caspase-8 activation in the hearts (45). It is noteworthy that autophagic cardiomyocyte death has been reported to be detectable more frequently than apoptosis or oncosis in failing or hemodynamically overloaded human hearts (3, 6, 7), although the frequency of the each form of cell death may be influenced by disease stages and backgrounds (*e.g.* age, etiology, clinical feature, and treatment) of the examined samples (2).

Recent studies have indicated a significant role of lysosomal cysteine and aspartic protease cathepsins in execution of ACD (21, 46). PC12 cells cultured in a serum-deprived condition showed morphological features characteristic of ACD with an increase in proteolytic activity of cathepsin D (46), and forced expression of cathepsin D in PC12-induced rapid cell death, indicating a regulatory role of cathepsin D in ACD. Expression of cathepsin D was increased in DT-treated TG hearts (Fig. 6*A*). In damaged cardiomyocytes, translocation of cathepsin D from lysosomes to the cytosol was evident, which is indicative of enhanced proteolytic activity (47). Cathepsin D has been reported to be activated in human failing hearts (5) and also to be a positive mediator of apoptotic cell death (22, 47). Further experiments are required to clarify whether cathepsin D is involved in execution of myocardial ACD in the pathogenesis of heart failure and how cathepsin D regulates these modes of cell death differentially.

According to the recent studies, ubiquitin-dependent protein degradation is linked to autophagy (48). Accumulation of ubiquitin in cardiomyocytes was observed in DT-treated TG hearts (Fig. 6*A*) as well as in human failing hearts (4, 6, 7). Kostin *et al.* (6) demonstrated a functional defect in the ubiquitin/proteasome pathway together with ubiquitin accumulation in human failing hearts, and speculated that an excess of ubiquitinated proteins might activate autophagic protein degradation. The precise molecular mechanisms of how ubiquitin accumulation enhances autophagy remain unknown, although ubiquitination is postulated to be required for maturation of autophagosomes (48). Unlike human failing hearts (6), the amounts of UBC2 and UFD1 were unchanged in the hearts of our model mice (Fig. 6*B*). Protein ubiquitination and deubiquitination are mediated by a large number of enzymes (49), and it is an important issue to be

addressed in the future how ubiquitin is accumulated in cardiomyocytes undergoing autophagic cell death.

Diphtheria is a communicable disease affecting the upper respiratory tract and occasionally the skin as primary infection (50). However, remote organs such as heart or peripheral nerves are often damaged when DT is absorbed into the systemic circulation. Although diphtheria infection has been rarely encountered in developed countries because of the high rates of vaccination after the mid 1960s, several sporadic outbreaks occurred, for example, in the former Union of Soviet Socialist Republics in 1990s (50). Myocardial involvement is a major complication that determines the prognosis, but the pathophysiology associated with diphtheritic cardiomyopathy remains largely unknown. Histological analysis of the postmortal heart of a diphtheria patient revealed hyaline degeneration of myocardium and infiltration of mononuclear cells, and cytosolic lipid droplets and clumped chromatin granules were observed by electron microscopic examination (51). Although vacuoles of autophagosomes were not described in this paper, these findings were similar to those observed in our mouse model. Interestingly, cardiomyocyte loss through ACD associated with a decrease in protein synthesis was also observed in anthracycline-induced cardiomyopathy (52). Therefore, autophagic cardiomyocyte death evoked by a decrease in protein synthesis might not be confined to diphtheritic cardiomyopathy, but a more generalized phenomenon that occurs during progression of heart failure arising from miscellaneous etiologies. In this regard, our model of experimentally induced heart failure will be useful to elucidate molecular mechanisms underlying structural and functional changes associated with ACD in heart failure.

Acknowledgments—We thank R. Kobayashi, E. Fujita, and M. Iida for excellent technical assistance. We are grateful to Dr. A. Ullrich (Max-Planck-Institute of Biochemistry, Martinsried, Germany) and Dr. J. Robbins (Children's Hospital, Cincinnati, OH) for providing cDNAs.

REFERENCES

1. Nadal, G. B., Kajstura, J., Leri, A., and Anversa, P. (2003) *Circ. Res.* **92,** 139–150
2. Kang, P. M., and Izumo, S. (2000) *Circ. Res.* **86,** 1107–1113
3. Yamamoto, S., Sawada, K., Shimomura, H., Kawamura, K., and James, T. N. (2000) *J. Mol. Cell Cardiol.* **32,** 161–175
4. Knaapen, M. W., Davies, M. J., De, B. M., Haven, A. J., Martinet, W., and Kockx, M. M. (2001) *Cardiovasc. Res.* **51,** 304–312
5. Shimomura, H., Terasaki, F., Hayashi, T., Kitaura, Y., Isomura, T., and Suma, H. (2001) *Jpn. Circ. J.* **65,** 965–968
6. Kostin, S., Pool, L., Elsasser, A., Hein, S., Drexler, H. C., Arnon, E., Hayakawa, Y., Zimmermann, R., Bauer, E., Klovekorn, W. P., and Schaper, J. (2003) *Circ. Res.* **92,** 715–724
7. Hein, S., Arnon, E., Kostin, S., Schonburg, M., Elsasser, A., Polyakova, V., Bauer, E. P., Klovekorn, W. P., and Schaper, J. (2003) *Circulation* **107,** 984–991
8. Mann, D. L. (1999) *Circulation* **100,** 999–1008
9. Schaper, J., Elsasser, A., and Kostin, S. (1999) *Circ. Res.* **85,** 867–869
10. Anversa, P. (2000) *Circ. Res.* **86,** 121–124
11. Pappenheimer, A. J. (1977) *Annu. Rev. Biochem.* **46,** 69–94
12. Falnes, P. O., and Sandvig, K. (2000) *Curr. Opin. Cell Biol.* **12,** 407–413
13. Van Ness, B. G., Howard, J. B., and Bodley, J. W. (1980) *J. Biol. Chem.* **255,** 10710–10716
14. Higashiyama, S., Abraham, J. A., Miller, J., Fiddes, J. C., and Klagsbrun, M. (1991) *Science* **251,** 936–939
15. Naglich, J. G., Metherall, J. E., Russell, D. W., and Eidels, L. (1992) *Cell* **69,** 1051–1061
16. Mitamura, T., Umata, T., Nakano, F., Shishido, Y., Toyoda, T., Itai, A., Kimura, H., and Mekada, E. (1997) *J. Biol. Chem.* **272,** 27084–27090
17. Saito, M., Iwawaki, T., Taya, C., Yonekawa, H., Noda, M., Inui, Y., Mekada, E., Kimata, Y., Tsuru, A., and Kohno, K. (2001) *Nat. Biotechnol.* **19,** 746–750
18. Kim, J., and Klionsky, D. J. (2000) *Annu. Rev. Biochem.* **69,** 303–342
19. Klionsky, D. J., and Emr, S. D. (2000) *Science* **290,** 1717–1721
20. Ohsumi, Y. (2001) *Nat. Rev. Mol. Cell. Biol.* **2,** 211–216
21. Bursch, W. (2001) *Cell Death Differ.* **8,** 569–581
22. Leist, M., and Jaattela, M. (2001) *Nat. Rev. Mol. Cell. Biol.* **2,** 589–598
23. Lockshin, R. A., and Zakeri, Z. (2002) *Curr. Opin. Cell Biol.* **14,** 727–733
24. Takano, H., Nagai, T., Asakawa, M., Toyozaki, T., Oka, T., Komuro, I., Saito, T., and Masuda, Y. (2000) *Circ. Res.* **87,** 596–602
25. Asakawa, M., Takano, H., Nagai, T., Uozumi, H., Hasegawa, H., Kubota, N., Saito, T., Masuda, Y., Kadowaki, T., and Komuro, I. (2002) *Circulation* **105,** 1240–1246
26. Toko, H., Zhu, W., Takimoto, E., Shiojima, I., Hiroi, Y., Zou, Y., Oka, T., Akazawa, H., Mizukami, M., Sakamoto, M., Terasaki, F., Kitaura, Y., Takano, H., Nagai, T., Nagai, R., and Komuro, I. (2002) *J. Biol. Chem.* **277,** 24735–24743
27. Akazawa, H., Komuro, I., Sugitani, Y., Yazaki, Y., Nagai, R., and Noda, T. (2000) *Genes Cells* **5,** 499–513
28. Vander, H. M., Chandel, N. S., Williamson, E. K., Schumacker, P. T., and Thompson, C. B. (1997) *Cell* **91,** 627–637
29. Saito, S., Hiroi, Y., Zou, Y., Aikawa, R., Toko, H., Shibasaki, F., Yazaki, Y., Nagai, R., and Komuro, I. (2000) *J. Biol. Chem.* **275,** 34528–34533
30. Chau, B. N., Borges, H. L., Chen, T. T., Masselli, A., Hunton, I. C., and Wang, J. Y. (2002) *Nat. Cell Biol.* **4,** 757–765
31. Komazaki, S., Ito, K., Takeshima, H., and Nakamura, H. (2002) *FEBS Lett.* **524,** 225–229
32. Komuro, I., and Yazaki, Y. (1993) *Annu. Rev. Physiol.* **55,** 55–75
33. Sadoshima, J., and Izumo, S. (1997) *Annu. Rev. Physiol.* **59,** 551–571
34. de Lemos, J. A., McGuire, D. K., and Drazner, M. H. (2003) *Lancet* **362,** 316–322
35. Mercadier, J. J., Lompre, A. M., Duc, P., Boheler, K. R., Fraysse, J. B., Wisnewsky, C., Allen, P. D., Komajda, M., and Schwartz, K. (1990) *J. Clin. Investig.* **85,** 305–309
36. Elsner, D., and Riegger, G. A. (1995) *Curr. Opin. Cardiol.* **10,** 253–259
37. Arber, S., Hunter, J. J., Ross, J. J., Hongo, M., Sansig, G., Borg, J., Perriard, J. C., Chien, K. R., and Caroni, P. (1997) *Cell* **88,** 393–403
38. Sussman, M. A., Welch, S., Cambon, N., Klevitsky, R., Hewett, T. E., Price, R., Witt, S. A., and Kimball, T. R. (1998) *J. Clin. Investig.* **101,** 51–61
39. Lee, P., Morley, G., Huang, Q., Fischer, A., Seiler, S., Horner, J. W., Factor, S., Vaidya, D., Jalife, J., and Fishman, G. I. (1998) *Proc. Natl. Acad. Sci. U. S. A.* **95,** 11371–11376
40. Anversa, P., Zhang, X., Li, P., and Capasso, J. (1992) *J. Clin. Investig.* **89,** 618–629
41. Lockshin, R. A., Osborne, B., and Zakeri, Z. (2000) *Cell Death Differ.* **7,** 2–7
42. Anglade, P., Vyas, S., Javoy-Agid, F., Herrero, M. T., Michel, P. P., Marquez, J., Mouatt-Prigent, A., Ruberg, M., Hirsch, E. C., and Agid, Y. (1997) *Histol. Histopathol.* **12,** 25–31
43. Kegel, K. B., Kim, M., Sapp, E., McIntyre, C., Castano, J. G., Aronin, N., and DiFiglia, M. (2000) *J. Neurosci.* **20,** 7268–7278
44. Cataldo, A. M., Hamilton, D. J., Barnett, J. L., Paskevich, P. A., and Nixon, R. A. (1996) *J. Neurosci.* **16,** 186–199
45. Wencker, D., Chandra, M., Nguyen, K., Miao, W., Garantziotis, S., Factor, S. M., Shirani, J., Armstrong, R. C., and Kitsis, R. N. (2003) *J. Clin. Investig.* **111,** 1497–1504
46. Uchiyama, Y. (2001) *Arch. Histol. Cytol.* **64,** 233–246
47. Roberg, K., and Ollinger, K. (1998) *Am. J. Pathol.* **152,** 1151–1156
48. Blommaart, E. F., Luiken, J. J., and Meijer, A. J. (1997) *Histochem. J.* **29,** 365–385
49. Pickart, C. M. (2004) *Cell* **116,** 181–190
50. Hadfield, T. L., McEvoy, P., Polotsky, Y., Tzinserling, V. A., and Yakovlev, A. A. (2000) *J. Infect. Dis.* **181,** Suppl. 1, S116–S120
51. Burch, G. E., Sun, S. C., Sohal, R. S., Chu, K. C., and Colcolough, H. L. (1968) *Am. J. Cardiol.* **21,** 261–268
52. Semenov, D. E., Lushnikova, E. L., and Nepomnyashchikh, L. M. (2001) *Bull. Exp. Biol. Med.* **131,** 505–510

THE JOURNAL OF CELL BIOLOGY

Katsuhisa Matsuura, Hiroshi Wada, Toshio Nagai, Yoshihiro Iijima, Tohru Minamino, Masanori Sano, Hiroshi Akazawa, Jeffery D. Molkentin, Hiroshi Kasanuki, and Issei Komuro

Vol. 167, No. 2, October 25, 2004. Pages 351–363.

A label (RFP$^+$ HUVEC) was left out of figure 2 B. The corrected figure appears below.

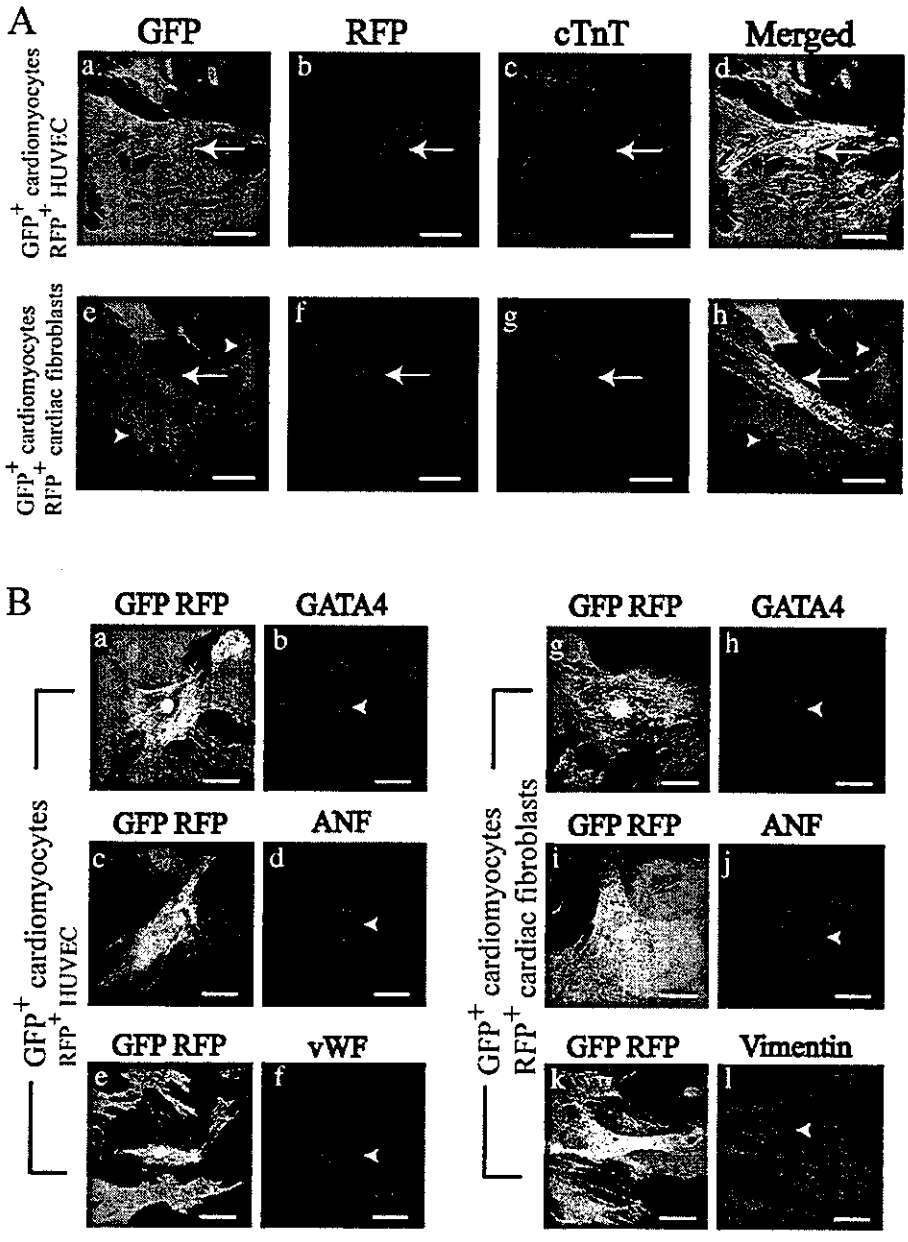

Case Report

Steroid-responsive thromboangiitis obliterans

Lancet 2004; 364: 1098

Atsuhiko T Naito, Tohru Minamino, Kaoru Tateno, Toshio Nagai, Issei Komuro

Department of Cardiovascular Science and Medicine (A T Naito MD, T Minamino MD, K Tateno MD, T Nagai MD, I Komuro MD) Chiba University Graduate School of Medicine, 1-8-1 Inohana, Chuo-ku, Chiba 260-8670, Japan

Correspondence to: Dr Issei Komuro komuro-tky@umin.ac.jp

A 41-year-old, non-smoking man came to the emergency room in June, 2003, complaining of cold, painful hands. On examination, we found nothing abnormal, apart from cyanotic, tender fingers, with poor perfusion as shown on by laser doppler and infrared thermography (figure). Blood tests showed eosinophilia; 3097/μL, and eosinophilic cationic protein (ECP), >150 μg/mL (normal <14·7 μg/mL). Acute-phase reactants, C-reactive protein and the erythrocyte sedimentation rate were within normal limits. Chest radiographs and echocardiography showed no abnormalities or evidence of eosinophilia-induced end-organ damage. Angiography showed occlusion of the distal arteries of upper and lower extremities. We searched for parasitic infections and malignancy, to no avail. We excluded vasculitis from our differential diagnosis when the results of immunological tests showed no antinuclear, anticentromere, anticardiolipin, anti-dsDNA, anti-Scl70, anti-SS-A, anti-RNP, and anti-Jo1 antibodies, rheumatoid factor, ANCA, or cryoglobulins. Serum tryptase level was low; 3·9 ng/mL, indicating no involvement of mast cells. Our patient thus fulfilled the Japanese criteria for thromboangiitis obliterans,[1,2] and we started treatment with intravenous heparin and alprostadil. The patient's digital ischaemia and intermittent claudication showed no improvement after 1 week and his middle finger became necrotic. At that point, his eosinophil count was 5014/μL. We decided to give him prednisolone 30 mg daily, to treat the eosinophilia, in case it was contributing to the distal arterial occlusion. After 2 weeks of treatment, his eosinophil count and serum ECP levels decreased to 185/mm³ and 19·5 μg/mL, respectively. Laser doppler and infrared thermography showed a clear improvement in digital ischaemia (figure). When last seen in April, 2004, his fingers were completely healed, and he had no complaints of claudication.

A 62-year-old non-smoking man had been diagnosed with thromboangiitis obliterans in October, 1997, on the basis of angiography that showed occlusion of distal arteries in the absence of atherosclerosis. For 6 years, he had been treated with beraprost, anti-coagulants, lumbar sympathetic block, and continuous epidural block, but digital necrosis and pain persisted. He was admitted to our hospital in September, 2003. Blood tests showed eosinophilia; 2300/μL and ECP; 107 μg/mL. Tests for other causes of vascuolopathy were negative. We treated him with prednisolone, 30 mg daily, and after 2 weeks, his eosinophil count was 185/mm³ and serum ECP was 25·8 μg/mL. His pain had disappeared and his digital ischaemia largely resolved by the time of discharge in December, 2003.

Both of these patients fulfilled the Japanese criteria for thromboangiitis obliterans, but they were atypical patients because they were non-smokers at the onset of the symptoms. Current history of smoking is included in many case definitions of thromboangiitis obliterans.[1] Stopping smoking is the only proven strategy to prevent the progression of this disease, but 6·8% of Japanese patients diagnosed with thromboangiitis obliterans are non-smokers.[2] Hypereosinophilia causes end-organ damage by inducing thrombosis and endothelial damage, and simultaneous presentations of thromboangiitis obliterans with eosinophilia due to temporal arteritis have been reported.[3,4] However, we could find no reports of distal artery occlusion consistent with thromboangiitis obliterans and eosinophilia that responded to steroids. It will be interesting to see if patients who are diagnosed with thromboangiitis obliterans include a subset that have steroid-responsive disease, mediated by eosinophilia.

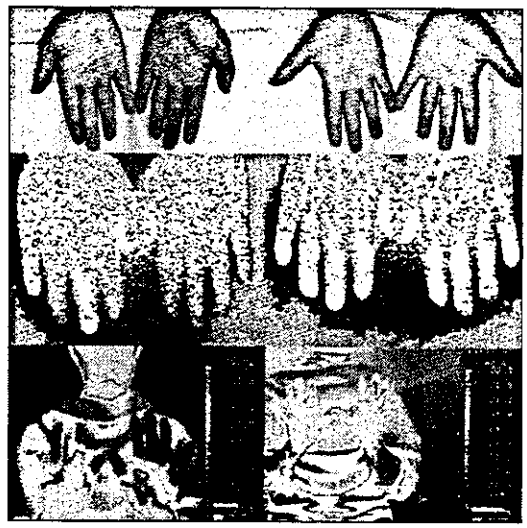

Figure: Photograph (top), laser doppler (middle), and infrared thermography (bottom), showing digital ischaemia before (left) and after steroid therapy (right).

References

1 Olin JW. Thromboangiitis obliterans (Buerger's disease). *N Engl J Med* 2000; 343: 864–69.

2 Sasaki S, Sakuma M, Yasuda K. Current status of thromboangiitis obliterans (Buerger's disease) in Japan. *Int J Cardiol* 2000; 75: S175–81.

3 Lie JT, Michet CJ Jr. Thromboangiitis obliterans with eosinophilia (Buerger's disease) of temporal arteries. *Hum Pathol* 1988; 19: 598–602.

4 Fujimoto M, Sato S, Hayashi N, Wakugawa M, Tsuchida T, Tamaki K. Juvenile temporal arteritis with eosinophilia: a distinct clinicopathological entity. *Dermatology* 1996; 192: 32–35.

5 Ferguson GT, Starkebaum G. Thromboangiitis obliterans associated with idiopathic hypereosinophilia. *Arch Intern Med* 1985; 145: 1726–28.

Available online at www.sciencedirect.com
SCIENCE DIRECT®
Biochemical and Biophysical Research Communications 325 (2004) 1353–1359
BBRC
www.elsevier.com/locate/ybbrc

Effects of G-CSF on cardiac remodeling after acute myocardial infarction in swine

Koji Iwanaga[a], Hiroyuki Takano[a], Masashi Ohtsuka[a], Hiroshi Hasegawa[a], Yunzeng Zou[a], Yingjie Qin[a], Kenichi Odaka[a], Kenzo Hiroshima[b], Hiroyuki Tadokoro[c], Issei Komuro[a,*]

[a] *Department of Cardiovascular Science and Medicine, Chiba University Graduate School of Medicine, Chiba, Japan*
[b] *Department of Basic Pathology, Chiba University Graduate School of Medicine, Chiba, Japan*
[c] *Division of Medical Imaging, National Institute of Radiological Science, Chiba, Japan*

Received 19 October 2004
Available online 11 November 2004

Abstract

We examined whether granulocyte colony-stimulating factor (G-CSF) prevents cardiac dysfunction and remodeling after myocardial infarction (MI) in large animals. MI was produced by ligation of left anterior descending coronary artery in swine. G-CSF (10 μg/kg/day, once a day) was injected subcutaneously from 24 h after ligation for 7 days. Echocardiographic examination revealed that the G-CSF treatment induced improvement of cardiac function and attenuation of cardiac remodeling at 4 weeks after MI. In the ischemic region, the number of apoptotic endothelial cells was smaller and the number of vessels was larger in the G-CSF treatment group than in control group. Moreover, vascular endothelial growth factor was more abundantly expressed and Akt was more strongly activated in the ischemic region of the G-CSF treatment group than of control group. These findings suggest that G-CSF prevents cardiac dysfunction and remodeling after MI in large animals.

Keywords: Akt; Angiogenesis; Apoptosis; Cytokine; G-CSF; Myocardial infarction; Remodeling; Swine; VEGF

Since left ventricular (LV) remodeling after myocardial infarction (MI) causes progression to heart failure, preventing the remodeling process following MI is an important therapeutic approach for heart failure. Although the therapeutic agents such as angiotensin converting enzyme inhibitors and β blockers prevent cardiac remodeling and reduce morbidity and mortality in patients with heart failure after MI, loss of cardiac myocytes could not be prevented by these agents. Although cardiac myocytes were previously considered as terminally differentiated cells, it has been recently reported that there are proliferating cardiac myocytes after MI in human hearts [1]. Moreover, it has been demonstrated that bone marrow stem cells (BMSCs) differentiate into cardiac myocytes, endothelial cells (ECs), and vascular smooth muscle cells (VSMCs) in adult mouse model of MI [2]. A highly enriched hematopoietic stem cell (HSC) population, so-called side population (SP), has also been reported to have the capacity to regenerate cardiac myocytes and blood vessels [3]. These studies suggest that locally delivered BMSCs or engrafted SP cells may generate new myocardium and then improve prognosis of patients with MI.

Granulocyte colony-stimulating factor (G-CSF) causes a marked increase in the release of HSCs and endothelial progenitor cells (EPCs) from bone marrow (BM) into the peripheral blood circulation, a process termed mobilization [4–7]. Recently, it has been reported that G-CSF improves cardiac function and reduces mortality after MI in mice [6–8]. The mobilized BM cells have been reported to differentiate into cardiac

* Corresponding author. Fax: +81 43 226 2557.
E-mail address: komuro-tky@umin.ac.jp (I. Komuro).

0006-291X/$ - see front matter © 2004 Elsevier Inc. All rights reserved.
doi:10.1016/j.bbrc.2004.10.149

myocytes, ECs, and VSMCs [6]. However, there have been reports indicating that transdifferentiation of BM cells into cardiomyocytes is very rare [7,8]. Thus, mechanisms by which G-CSF ameliorates cardiac dysfunction are not fully understood. In the present study, we examined as a preclinical study whether G-CSF treatment is effective in preventing cardiac remodeling after MI also in large animals and investigated the mechanism of beneficial effects of G-CSF.

Materials and methods

Swine MI model. Male Yorkshire swine (Science Breeding Farm, Iwate, Japan) weighing 15–20 kg were used to induce myocardial infarction. After opening the chest, permanent occlusion was created between the first and second diagonal branches of the left anterior descending coronary artery (LAD) with a 3-0 nylon surgical suture. The mortality during operation was approximately 20% in this study. All the cause of death was arrhythmia (ventricular tachycardia and ventricular fibrillation). Since we used the swine which had not suffered arrhythmia, the swine were not treated with electrical defibrillation. All protocol was approved by the Institutional Animal Care and Use Committee of the Chiba University.

Cytokine treatment. The swine were randomized into two groups. (1) G-CSF treatment group ($n = 10$); injected subcutaneously with recombinant human G-CSF (10 μg/kg/day, Kirin Brewery, Tokyo, Japan), (2) control group ($n = 10$); injected subcutaneously with saline as the same volume as G-CSF, beginning at 24 h after MI and continuning daily for 7 days. The numbers of circulating white blood cells (WBC) and granulocytes were counted before and at 1, 3, 5, 7, and 28 days after MI. By using myocardial contrast echocardiography (MCE) analysis, we confirmed every time before the permanent ligation of LAD that the extent of area at risk (AAR) was constant. After that, an investigator, who was different from operators, randomized the swine into two groups. The measurement of echocardiography and the estimation of pathology were performed by other persons blinded to randomization. Moreover, we measured the serum levels of creatine kinase-MB isoenzyme (CK-MB) and cardiac troponin I (cTnI) at the earlier time points after MI in both G-CSF treatment group and control group.

Physiological analysis. Echocardiographic studies were performed at pre-operation and 4 weeks after LAD ligation with an Philips Sonos 5500 and an ultraband S4 sector transducer. The transducer was placed on a standoff positioned on the epicardium. LV end-diastolic area (LVAd), LV end-systolic area (LVAs), diastolic interventricular septum wall thickness (IVSTd), diastolic LV posterior wall thickness (PWTd), and fractional area change (FAC) at the level of mid papillary muscles in short-axis view were measured by B-mode. MCE was performed with contrast agent (Levovist, Nihon Schering, 300 mg/10 s).

Histological analysis. Four weeks after MI, triphenyltetrazolium chloride (TTC) staining was performed to estimate infarct size. The heart was cut into six transverse slices, and one slice containing the mid papillary muscle was incubated for 5 min at 37 °C in 1% solution of TTC. The infarcted (pale) and viable (red) myocardium were measured by computed planimetry (NIH IMAGE 1.63, NIH, ML). Infarct size measured from tracing of myocardial slices was calculated as a percentage of LV area. Cardiomyocytes were identified immunohistochemically using anti-cardiac troponin T (cTnT) antibody (Santa Cruz Biotechnology, CA). Endothelial cells were identified immunohistochemically using anti-von Willebrand factor (vWF) antibody (Dako, CA) and smooth muscle cells were identified by anti-α-smooth muscle actin antibody (Dako, CA). Expressions of cTnT and vWF were visualized by Cy3-labeled secondary antibody. To count the numbers of vessels, 15 fields were randomly chosen from remote (non-infarct), border (ischemia), and infarct regions in each sample ($n = 10$, each groups). For detection of apoptotic cells, TUNEL assay was performed using In situ Apoptosis Detection Kit (Takara, Japan). To identify which cells were TUNEL-positive, we further performed double-staining by using anti-cTnT or anti-vWF antibody with TUNEL assay.

Western blot analysis. Four weeks after MI, whole tissue lysates were extracted from hearts and subjected to Western blot analysis. The extracts were centrifuged at 14,000 rpm at 4 °C for 30 min, and the total protein concentration was measured with the BCA protein assay kit (Pierce, IL). Proteins (50 μg) were separated in 10–15% SDS–PAGE and transferred onto a nitrocellulose transfer membrane (Schleicher & Schuell, Netherlands). After blocking in TBS-T (150 mmol/L NaCl, 50 mmol/L Tris, and 0.1% Tween 20, pH 7.4) containing 5% skim milk, the membranes were incubated with antibodies against Akt1, phospho-Akt1, or VEGF (Santa Cruz Biotechnology, CA). VEGF blocking peptide was used to identify the band of VEGF. Hybridizing bands were visualized using an ECL detecting kit (Amersham–Pharmacia Biotech, NJ). The equal loading was validated by staining with Ponceau S.

Statistical analysis. All data are presented as means ± SD. All data were analyzed by one-way ANOVA followed by the Bonferroni procedure for comparison of means. A probability value of $P < 0.05$ was considered to be statistically significant.

Results

Blood collection and laboratory analysis

Blood samples were collected before and at 1, 3, 5, 7, and 28 days after MI with or without G-CSF treatment (Figs. 1A and B). Although there was no significant difference in their numbers between G-CSF treatment group and control group at pre-operation, both numbers were significantly larger in G-CSF treatment group (WBC, 55,500 ± 16,426/mm^3; granulocytes, 41,352 ± 14,791/mm^3) than in control group (WBC, 21,000 ± 7867/mm^3, granulocytes, 10,932 ± 6827/mm^3) at 3 days after MI (Figs. 1A and B). Plasma G-CSF concentration was not detectable at pre-operation in both groups and was increased at 1 week after MI in control group (192 ± 1.4 pg/mL). G-CSF concentration was much higher in G-CSF treatment group (1980 ± 867 pg/mL) than in control group, suggesting that subcutaneously injected G-CSF (10 μg/kg/day) was enough to induce mobilization in swine model. We next evaluated the size of infarction in both groups by measuring the serum levels of CK-MB and cTnI. Since there were no significant differences in the levels of CK-MB and cTnI between control group and the G-CSF treatment group at the any time after MI, the initial infarct size of both groups seemed to be same (Figs. 1C and D).

Echocardiographic analysis

We evaluated cardiac function and LV remodeling by echocardiography at pre-operation and 4 weeks after MI (Table 1). At pre-operation there was no significant

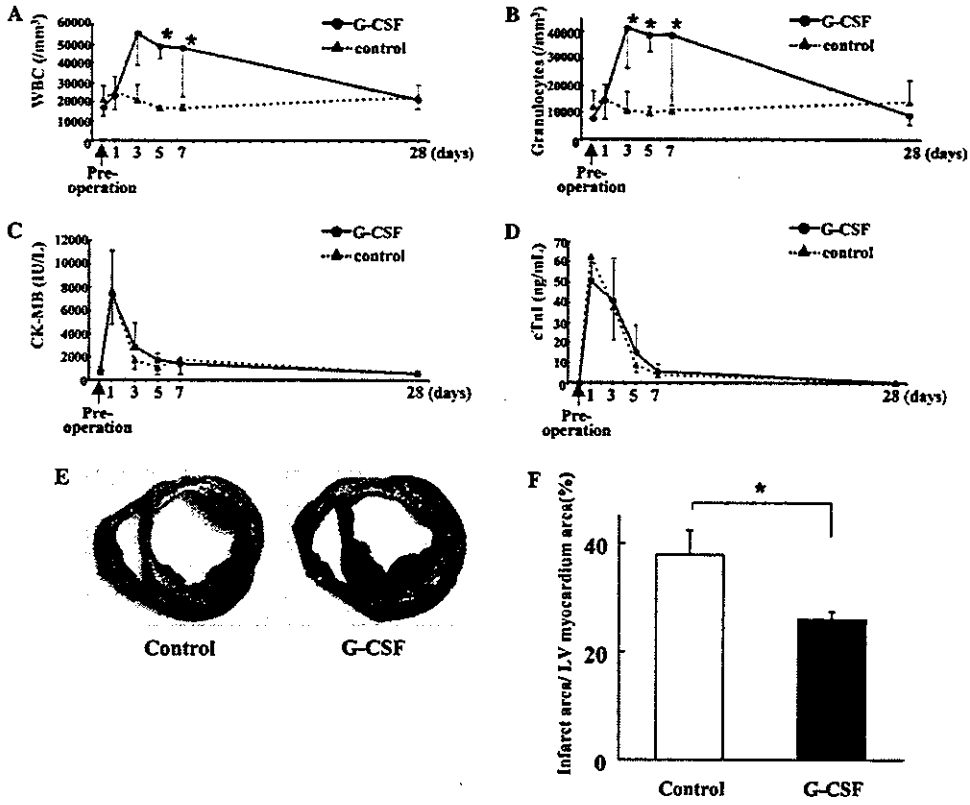

Fig. 1. Histological analysis. (A,B) The number of circulating white blood cells (WBC) and granulocytes was counted at pre-operation, 1, 3, 5, 7, and 28 days after MI. (C) Serum levels of creatine kinase-MB isozyme (CK-MB) were measured at pre-operation, 1, 3, 5, 7, and 28 days after MI. (D) Serum levels of cardiac troponin I (cTnI) were measured at pre-operation, 1, 3, 5, 7, and 28 days after MI. There was no significant difference in CK-MB and cTnI levels between control group and the G-CSF treatment group at any time after MI. (E) Triphenyltetrazolium chloride (TTC) staining. The area of infarcted (pale) and viable (red) myocardium was measured by computed planimetry. (F) Infarct size measured from tracing of myocardial slices was calculated as a percentage of LV area. Infarct size was much smaller in the G-CSF treatment group than in control group. Results are given as means ± SD ($n = 10$). *$P < 0.05$.

Table 1
Echocardiographic parameters measured before and 4 weeks after MI

	IVSTd (mm)		PWTd (mm)		LVAd (cm^2)		LVAs (cm^2)		FAC (%)	
	Pre-MI	4w	Pre-MI	4w	Pre-MI	4w	Pre-MI	4w	Pre-MI	4w
Control	6.1 ± 1.1	3.5 ± 0.4	6.3 ± 0.8	7.5 ± 1.0	8.1 ± 1.0	17.6 ± 2.1	5.1 ± 0.7	12.4 ± 2.9	37.5 ± 8.0	18.1 ± 4.0
G-CSF	6.1 ± 1.1	5.1 ± 1.0*	6.4 ± 0.9	6.3 ± 0.9*	8.4 ± 1.4	12.5 ± 1.7*	5.1 ± 0.9	8.1 ± 0.6*	38.7 ± 10.7	29.6 ± 5.4*

IVSTd, interventricular septum wall thickness at diastole; PWTd, LV posterior wall thickness at diastole; LVAd, LV end-diastolic area; LVAs, LV end-systolic area; and FAC; fractional area change.
* $P < 0.05$ vs control.

difference in cardiac performance between control group (IVSTd, 6.1 ± 1.1 mm; PWTd, 6.3 ± 0.8 mm; LVAd, 8.1 ± 1.0 cm^2; LVAs, 5.1 ± 0.7 cm^2; and FAC, 37.5 ± 8.0%) and the G-CSF-treatment group (IVSTd, 6.1 ± 1.1 mm; PWTd, 6.4 ± 0.9 mm; LVAd, 8.4 ± 1.4 cm^2; LVAs, 5.1 ± 0.9 cm^2; and FAC, 38.7 ± 10.7%). The change of these parameters became more prominent in control group at 4 weeks after MI (IVSTd, 3.5 ± 0.4 mm; PWTd, 7.5 ± 1.0 mm; LVAd, 17.6 ± 2.1 cm^2; LVAs, 12.4 ± 2.9 cm^2; and FAC, 18.1 ± 4.0%) but not in the G-CSF group (IVSTd, 5.1 ± 1.0 mm; PWTd, 6.3 ± 0.9 mm; LVAd, 12.5 ± 1.7 cm^2; LVAs, 8.1 ± 0.6 cm^2; and FAC, 29.6 ± 5.4%) (Table 1).

Infarct size

Gross anatomical examination revealed that the LV wall thickness at MI region was very thin and the LV

cavity was markedly expanded in control group but not the G-CSF treatment group. TTC staining revealed that infarct area/LV myocardium area (%) was significantly less in the G-CSF treatment group than in control group (Figs. 1E and F).

Neovascularization

To clarify the mechanisms by which G-CSF improves LV remodeling and dysfunction after MI, we first examined the number of vessels because it has been reported that injection of BM cells into the heart after MI prevents the remodeling through angiogenesis and that G-CSF induces mobilization of EPCs [6–9]. In both border and infarct regions, there were more vWF-positive vessels in the G-CSF treatment group than in control group (Figs. 2A and B). These results suggest that G-CSF may ameliorate myocardial perfusion at least in part through an increase in the numbers of vessels.

Apoptotic cells

It has been reported that apoptotic cell death contributes to expansion of MI extent and progression of LV remodeling after MI [10]. We thus measured the number

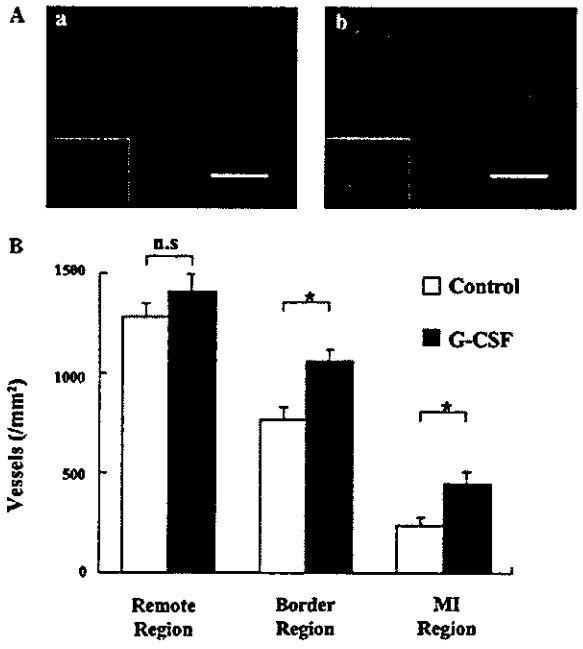

Fig. 2. Vessel analysis. (A) Endothelial cells of border zone myocardium were identified immunohistochemically using anti-von Willebrand factor (vWF) antibody (a, control group; b, G-CSF group), (magnification 100×, scale bar, 200 μm; magnification 400×, insets). (B) To measure the number of vessels, 15 fields were randomly chosen from remote, border, and MI regions in each sample ($n = 10$, each groups). Results are given as means ± SD ($n = 10$). *$P < 0.05$.

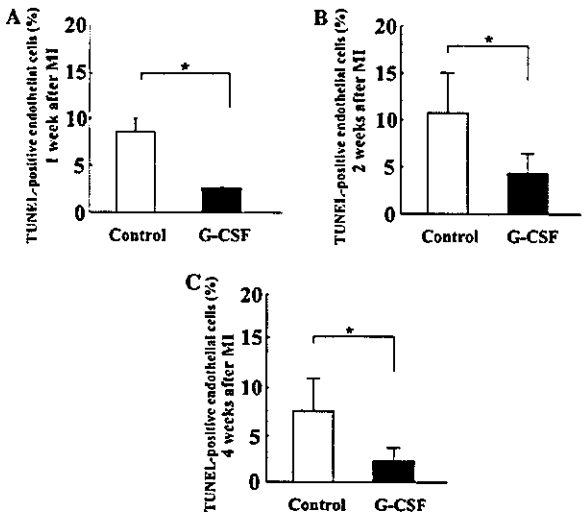

Fig. 3. Apoptotic cell death. The number of TUNEL-positive ECs was significantly smaller in the G-CSF treatment group than in control group at 1 week (A), 2 weeks (B), and 4 weeks (C), respectively. Results are given as means ± SD ($n = 10$). *$P < 0.05$.

of apoptotic cells using TUNEL assay in the border region of MI heart. The number of TUNEL-positive cells in the border region was markedly smaller in the G-CSF treatment group (2 weeks, $3.3 \pm 1.5/10^3$ cells; 4 weeks, $5.6 \pm 2.1/10^3$ cells) than that in control group (2 weeks, $10.7 \pm 3.2/10^3$cells; 4 weeks, $12.6 \pm 4.7/10^3$cells). Very few apoptotic cardiomyocytes were recognized at all time points examined. Most of TUNEL-positive cells were infiltrated blood cells and a part of TUNEL-positive cells were vascular cells. To identify apoptotic cells, we performed double-staining using anti-vWF antibody and TUNEL. Almost all vascular cells positive for TUNEL expressed vWF, suggesting that apoptotic cells in the vessel are ECs. The number of TUNEL-positive ECs was significantly smaller in the G-CSF treatment group (1 week, $2.3 \pm 0.1\%$; 2 weeks, $4.2 \pm 1.9\%$; and 4 weeks, $2.6 \pm 2.1\%$) than in control group (1 week, $8.2 \pm 1.3\%$; 2 weeks, $11.0 \pm 4.4\%$; and 4 weeks, $8.1 \pm 3.9\%$) (Figs. 3A–C).

Akt and VEGF

Since Akt has been reported to play an important role in cell survival and angiogenesis [11], we next examined the activity of Akt. Western blot analysis demonstrated that the phosphorylated Akt1 was decreased markedly in the MI region and moderately in the border region (Figs. 4A and B). The G-CSF treatment increased the activity of Akt1 in all regions (Figs. 4A and B). VEGF is a member of angiogenic growth factor family and induces proliferation and survival of ECs [12]. The expression of VEGF protein was markedly

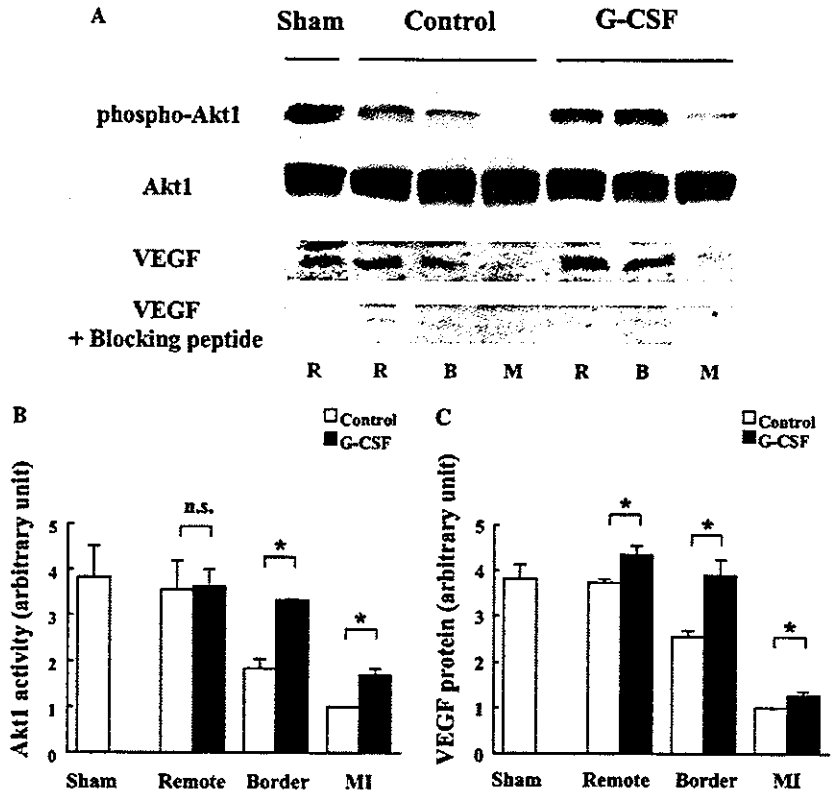

Fig. 4. Akt1 activity and VEGF protein level in myocardium. (A) Four weeks after MI, whole tissue lysates were extracted from hearts of three regions such as remote region, border region, and MI region, and subjected to Western blot analysis. The membranes were incubated with antibodies against Akt1, phospho-Akt1 or VEGF. VEGF blocking peptide was used to identify the band of VEGF. Results are representative of five independent experiments. R, remote region; B, border region; and M, MI region. (B,C) Quantitative analysis of phospho-Akt1 (B) and VEGF (C). Equal loading was validated by Ponceau S staining. Results are given as means ± SD ($n = 5$). *$P < 0.05$.

downregulated in the MI region (Figs. 4A and C). Downregulation of VEGF protein in the border region was milder in the G-CSF treatment group than in control group (Figs. 4A and C).

Discussion

In the present study, the G-CSF treatment prevented cardiac remodeling after MI in a preclinical swine model. The G-CSF treatment decreased apoptotic death of ECs and increased the number of vessels at the ischemic region, resulting in reduction in the infarcted size. G-CSF-induced activation of Akt and upregulation of VEGF may be associated with the beneficial effects.

Recently, BMSCs have been expected as the potential tool in regenerative medicine. Orlic et al. [2] have demonstrated that direct injection of BMSCs into the MI heart improves the cardiac function and mortality. Kamihata et al. [13] injected BM-derived mononuclear cells into the ischemic border and infarcted zone immediately after MI in pig, and demonstrated that myocardial blood flow was improved 3 weeks later. Moreover, Orlic et al. [6] examined whether treatment with cytokines increases mobilization of BMSCs to injured myocardium and promotes myocardial regeneration. After injection with rat stem cell factor (SCF) and recombinant human G-CSF once a day for 5 days, mice were subjected to ligation of left coronary artery. SCF and G-CSF were given for 3 more days. Cytokine-mediated mobilization of BM cells resulted in myocardial regeneration characterized by dividing cardiac myocytes and forming vascular structures 27 days after MI [6]. The treatment significantly improved cardiac function and reduced mortality. These results suggest that mobilized adult BMSCs transdifferentiate into cardiac myocytes, ECs, and VSMCs in ischemic myocardium and that cytokine therapy can be a noninvasive therapeutic strategy for regeneration of myocardium. However, their cytokine treatment was started before MI, and thus it is not clinically applicable. To elucidate whether the cytokine therapy can be clinically applied, we first examined whether subcutaneous injection of G-CSF, which is started from 24 h after

MI, has beneficial effects on cardiac function and cardiac remodeling in mice [8]. The G-CSF treatment started after MI was as effective as the pretreatment [8]. We next examined here as a preclinical study whether G-CSF treatment after MI prevents LV remodeling and improves cardiac function in large animals.

G-CSF has been reported to induce mobilization of BMSCs and EPCs as well as increase circulating WBC and granulocytes [14]. We first measured the numbers of WBC and granulocytes before and at 1, 3, 5, 7, and 28 days after MI in both G-CSF group and control group. The numbers of WBC and granulocytes were significantly increased in the G-CSF group. Although it remains unknown whether the increase in circulating WBC is associated with the prevention of LV remodeling after MI, BMSCs, and EPCs, whose mobilization could be induced by G-CSF, may be involved in cardiac regeneration and neovascularization [2,3,7,8,15].

The number of vessels in both ischemic and infarct regions was larger in the G-CSF treatment group than in control group. We have recently reported that the G-CSF treatment induces mobilization of BM cells into the infarct heart and that the BM cells are involved in an increase in vessel number [8]. In this study, we observed that the G-CSF treatment decreased the number of apoptotic ECs. On the other hand, we could not detect apoptotic cardiomyocytes in hearts at 2 days, 1 week, and 2 weeks after MI by double-staining with cTnT and TUNEL. Most of TUNEL-positive cells were infiltrated blood cells and a part of TUNEL-positive cells were observed at ECs. Although we could not demonstrate that G-CSF inhibits an increase in apoptotic cardiomyocytes after MI, our results suggest that G-CSF-induced increase in vessel number by a decrease in apoptotic vascular cells may prevent cardiomyocyte death after MI, resulting in the reduction of infarct size. It has been reported that G-CSF receptors exist in ECs and that G-CSF activates signal transduction pathways such as Jak/STAT and MAPK family in ECs [16,17]. Activation of Jak/STAT and ERK is known to induce survival through upregulating anti-apoptotic molecules including bcl-2 and bcl-xL. Although we have not examined whether G-CSF directly acts on ECs after MI, there is a possibility that G-CSF may directly prevent apoptosis of ECs by activating the survival signal pathways. To elucidate the mechanism of how the G-CSF treatment prevents LV remodeling after MI, we examined the expression of VEGF, a major member of angiogenic and survival growth factor family [12], in the myocardium after MI. The expression of VEGF in the ischemic region was more abundant in the G-CSF treatment group than in control group. G-CSF has been reported to activate a variety of intracellular signaling cascades such as Jak/STAT, Ras/Raf/MAP kinase, and Src family kinase pathways [14]. We have recently examined whether G-CSF acts directly on neonatal rat cardiomyocytes in vitro. Our results demonstrated that G-CSF induces an increase in expression levels of VEGF through Jak2/STAT3 pathway in cardiomyocytes (unpublished data). In nonproliferating terminally differentiated cells, G-CSF has been reported to activate the PI3K/Akt pathway [18]. Akt has been reported to play a critical role in cell survival and angiogenesis [11]. Furthermore, Mangi et al. [19] reported that Akt1 prevents remodeling and nearly normalizes cardiac performance. The G-CSF treatment increased the activity of Akt1 in the border region. Moreover, we recently found that G-CSF increases Akt1 activity in cardiac myocytes (unpublished data). Therefore, activation of Akt1 in the heart may indicate the activation of Akt1 in cardiomyocytes.

The patients with acute MI generally undergo percutaneous coronary intervention if the patients are hospitalized within the golden time. Therefore, the beneficial effects of G-CSF observed in the present study may be limited to the patients who do not undergo reperfusion. Further studies are needed to elucidate the cardioprotective effects of G-CSF on myocardial ischemia/reperfusion model.

Acknowledgments

The authors thank E. Fujita, R. Kobayashi, M. Watanabe, and Y. Ohtsuki for excellent technical assistance. This work was supported by a Grant-in-Aid for Scientific Research, Developmental Scientific Research, and Scientific Research on Priority Areas from the Ministry of Education, Science, Sports and Culture, and by the Program for Promotion of Fundamental Studies in Health Sciences of the Organization for Drug ADR Relief, R&D Promotion and Product Review of Japan (to I. Komuro).

References

[1] A.P. Beltrami, K. Urbanek, J. Kajstura, S.M. Yan, N. Finato, R. Bussani, B. Nadal-Ginard, F. Silvestri, A. Leri, C.A. Beltrami, P. Anversa, Evidence that human cardiac myocytes divide after myocardial infarction, N. Engl. J. Med. 344 (2001) 1750–1757.

[2] D. Orlic, J. Kajstura, S. Chimenti, I. Jakoniuk, S.M. Anderson, B. Li, J. Pickel, R. McKay, B. Nadal-Ginard, D.M. Bodine, A. Leri, P. Anversa, Bone marrow cells regenerate infarcted myocardium, Nature 410 (2001) 701–705.

[3] K.A. Jackson, S.M. Majka, H. Wang, J. Pocius, C.J. Hartley, M.W. Majesky, M.L. Entman, L.H. Michael, K.K. Hirschi, M.A. Goodell, Regeneration of ischemic cardiac muscle and vascular endothelium by adult stem cells, J. Clin. Invest. 107 (2001) 1395–1402.

[4] L.B. To, D.N. Haylock, P.J. Simmons, C.A. Juttner, The biology and clinical uses of blood stem cells, Blood 89 (1997) 2233–2258.

[5] D.C. Link, Mechanisms of granulocyte colony-stimulating factor-induced hematopoietic progenitor-cell mobilization, Semin. Hematol. 37 (2000) 25–32.

[6] D. Orlic, J. Kajstura, S. Chimenti, F. Limana, I. Jakoniuk, F. Quaini, B. Nadal-Ginard, D.M. Bodine, A. Leri, P. Anversa, Mobilized bone marrow cells repair the infarcted heart, improving function and survival, Proc. Natl. Acad. Sci. USA 98 (2001) 10344–10349.

[7] A.A. Kocher, M.D. Schuster, M.J. Szabolcs, S. Takuma, D. Burkhoff, J. Wang, S. Homma, N.M. Edwards, S. Itescu, Neovascularization of ischemic myocardium by human bone-marrow-derived angioblasts prevents cardiomyocyte apoptosis, reduces remodeling and improves cardiac function, Nat. Med. 7 (2001) 430–436.

[8] M. Ohtsuka, H. Takano, Y. Zou, H. Toko, H. Akazawa, Y. Qin, M. Suzuki, H. Hasegawa, H. Nakaya, I. Komuro, Cytokine therapy prevents left ventricular remodeling and dysfunction after myocardial infarction through neovascularization, FASEB J. 18 (2004) 851–853.

[9] T. Asahara, H. Masuda, T. Takahashi, C. Kalka, C. Pastore, M. Silver, M. Kearne, M. Magner, J.M. Isner, Bone marrow origin of endothelial progenitor cells responsible for postnatal vasculogenesis in physiological and pathological neovascularization, Circ. Res. 85 (1999) 221–228.

[10] A. Abbate, G.G.L. Biondi-Zoccai, A. Baldi, Pathophysiologic role of myocardial apoptosis in post-infarction left ventricular remodeling, J. Cell. Physiol. 193 (2002) 1243–1250.

[11] I. Shiojima, K. Walsh, Role of Akt signaling in vascular homeostasis and angiogenesis, Circ. Res. 90 (2002) 1243–1250.

[12] N. Ferrara, Role of vascular endothelial growth factor in regulation of physiological angiogenesis, Am. J. Physiol. Cell Physiol. 280 (2001) C1358–C1366.

[13] H. Kamihata, H. Matsubara, T. Nishiue, S. Fujiyama, Y. Tsutsumi, R. Ozono, H. Masaki, Y. Mori, O. Iba, E. Tateishi, A. Kosaki, S. Shintani, T. Murohara, T. Imaizumi, T. Iwasaka, Implantation of bone marrow mononuclear cells into ischemic myocardium enhances collateral perfusion and regional function via side supply of angioblasts, angiogenic ligands, and cytokines, Circulation 104 (2001) 1046–1052.

[14] B.R. Avalos, Molecular analysis of the granulocyte colony-stimulating factor receptor, Blood 88 (1996) 761–777.

[15] T. Takahashi, C. Kalka, H. Masuda, D. Chen, M. Silver, M. Kearney, M. Magner, J.M. Isner, T. Asahara, Ischemia- and cytokine-induced mobilization of bone marrow-derived endothelial progenitor cells for neovascularization, Nat. Med. 5 (1999) 434–438.

[16] E. Bocchietto, A. Guglielmetti, F. Silvagno, G. Taraboletti, G.P. Pescarmona, A. Mantovani, F. Bussolino, Proliferative and migratory responses of murine microvascular endothelial cells to granulocyte colony-stimulating factor, J. Cell. Physiol. 155 (1993) 89–95.

[17] B. Fuste, R. Mazzara, G. Escolar, A. Merino, A. Ordinas, M. Diaz-Ricart, Granulocyte colony-stimulating factor increases expression of adhesion receptors on endothelial cells through activation of p38 MAPK, Haematologica 89 (2004) 578–585.

[18] F. Dong, A.C. Larner, Activation of Akt kinase by granulocyte colony-stimulating factor (G-CSF): evidence for the role of a tyrosine kinase activity distinct from the janus kinases, Blood 95 (2000) 1656–1662.

[19] A.A. Mangi, N. Noiseux, D. Kong, H. He, M. Rezvani, J.S. Ingwall, V.J. Dzau, Mesenchymal stem cells modified with Akt prevent remodeling and restore performance of infarcted hearts, Nat. Med. 9 (2003) 1195–1201.

J Pharmacol Sci 96, 23 – 26 (2004)

Journal of Pharmacological Sciences

Forum Minireview

Forefront of Na^+/Ca^{2+} Exchanger Studies: Role of Na^+/Ca^{2+} Exchanger – Lessons From Knockout Mice

Issei Komuro[1,*] and Masashi Ohtsuka[1]

[1]*Department of Cardiovascular Science and Medicine, Chiba University Graduate School of Medicine, 1-8-1 Inohana, Chuo-ku, Chiba 260-8670, Japan*

Received June 14, 2004; Accepted July 27, 2004

Abstract. We used Na^+/Ca^{2+} exchanger (NCX) knockout mice to evaluate the effects of NCX in cardiac function and the infarct size after ischemia/reperfusion injury. The contractile function in NCX KO mice hearts was significantly better than that in wild type (WT) mouse hearts after ischemia/reperfusion and the infracted size was significantly smaller in NCX KO mice hearts compared with that in WT mice hearts. NCX is critically involved in the development of ischemia/reperfusion-induced myocardial injury, and therefore the inhibition of NCX function may contribute to cardioprotection against ischemia/reperfusion injury.

Keywords: Na^+/Ca^{2+} exchanger (NCX), knockout mouse, heart, ischemia/reperfusion injury

Introduction

The Na^+/Ca^{2+} exchanger (NCX) is an important electrogenic transporter in maintaining calcium homeostasis in a variety of mammalian organs (1). NCX catalyzes electrogenic exchange of Na^+ and Ca^{2+} across the plasma membrane in either the Ca^{2+}-efflux (the forward mode) or Ca^{2+}-influx (the reverse mode), depending on the electrochemical gradients of the substrate ions. In the heart, NCX plays an important role in excitation-contraction coupling as the dominant myocardial Ca^{2+}-efflux system (2). On the other hand, the reverse mode of NCX is associated with in cytoplasmic Ca^{2+} levels in cardiomyocytes during digitalis treatment or ischemia/reperfusion (3). It has been reported that NCX inhibitors and NCX antisense oligonucleotides protect the heart from ischemia/reperfusion injury (4, 5). However, two putative NCX inhibitors, KB-R7943 and SEA0400, have been reported to be not specific for NCX (6). Therefore, it remains unclear whether NCX indeed plays a crucial role in mediating Ca^{2+} influx that leads to Ca^{2+} overload and cellular injury after myocardial ischemia, reperfusion injury.

We generated *Ncx1*-deficient mice by gene targeting to determine the in vivo function of the exchanger (7). Homozygous *Ncx1*-deficient mice died between embryonic days 9 and 10. Their hearts did not beat, and cardiac myocytes showed apoptosis. No forward mode or reverse mode of the Na^+/Ca^{2+} exchange activity was detected in null mutant hearts. The Na^+-dependent Ca^{2+} exchange activity as well as protein content of NCX1 were decreased by approximately 50% in the heart, kidney, aorta, and smooth muscle cells of the heterozygous mice, and tension development of the aortic ring in Na^+-free solution was markedly impaired in heterozygous mice. These findings suggest that NCX1 is required for heartbeats and survival of cardiac myocytes in embryos and plays critical roles in Na^+-dependent Ca^{2+} handling in the heart and aorta.

*Corresponding author. FAX: +81-43-226-2557
E-mail: komuro-tky@umin.ac.jp

The functional activity as well as the protein content of NCX in the myocardium of NCX KO mice is approximately half of those of WT mice

Twelve-week-old male heterozygous knockout (KO) mice and wild type (WT) littermates were used. All animal experiments were performed according to the Guide for the Care and Use of Laboratory Animals (NIH publication No. 85-23, revised 1996). Ventricular cells were prepared from adult mouse hearts by standard enzymatic digestion (8). Whole-cell membrane currents were recorded by the patch-clamp method and the current-voltage relationship was obtained by voltage clamp ramp pulses as described previously (9). Under

these conditions, the Ni^{2+}-sensitive current represents NCX current (10). All data were acquired and analyzed by the pCLAMP (version 5.5; Axon Instrument) software.

Expression levels of dihydropyridine (DHP) receptor (L-type Ca^{2+} channel) and SR Ca^{2+}-ATPase 2 (SERCA2) were analyzed by Western blot as described previously (11). Briefly, tissue was homogenized in lysis buffer containing 25 mM Tris-HCl (pH 7.4), 25 mM NaCl, 0.5 mM EGTA, 10 mM sodium pyrophosphate, 1 mM sodium orthovanadate, 10 mM NaF, 10 nM okadaic acid, 1 mM PMSF, 20 μg/ml aprotinin, and 20 μg/ml leupeptin. Protein concentration was determined using a protein assay kit (BioRad, Hercules, CA, USA) and equal amounts of total protein (40 μg/lane) were separated on 8% SDS-polyacrylamide gel. Separated proteins were transferred to nitrocellulose membrane (Amersham Life Science, Arlington Heights, IL, USA). Membranes were incubated with anti-mouse dihydropyridine L-type Ca^{2+} channel α-2 subunit monoclonal antibody (Affinity Bioreagents, Inc., Golden, CO, USA) or anti-mouse SERCA2 monoclonal antibody (Affinity Bioreagents) at 4°C overnight. After washing, the membranes were incubated with horseradish peroxidase-conjugated goat anti-mouse antibody for 1 h. Immunoreactive protein was visualized using an enhanced chemiluminescence detection kit (ECL, Amersham).

We previously reported that the protein content of NCX in NCX KO mouse hearts was approximately 50% of that in WT mouse hearts (12). To elucidate the functional activity, we examined NCX current densites from −40 mV to 40 mV in WT (n = 9) and NCX KO ventricular cells (n = 6) (Fig. 1). The densities of the reverse mode of NCX at 40 mV in ventricular cells of KO mice (0.57 ± 0.07 pA/pF) were approximately half (55.4%) compared with those of WT mice (1.04 ± 0.14 pA/pF). These results suggest that the functional activity as well as the protein content of NCX in the myocardium of NCX KO mice is approximately half of those of WT mice.

Western blot analysis revealed that there was no difference in the protein levels of L-type Ca^{2+} channel and SERCA2 between the two groups (data not shown).

The infarct size was significantly smaller in KO hearts than in WT hearts

Hearts were excised from mice and connected to the perfusion canula via the aorta as described previously (8). Retrograde perfusion was maintained with Krebs-Henseleit solution. To evaluate the contractile function, a polyethylene film balloon was inserted into the cavity of the left ventricle through the left atrium. The balloon was filled with saline to adjust the baseline end-diastolic pressure to 5 – 10 mmHg. Hearts were subjected to no-flow, global ischemia by clamping the perfusion line. After 30 min of ischemia, the clamp was released and the hearts were reperfused for 120 min. Left ventricular developed pressure (LVDP) was designated as difference between systolic and diastolic pressures of the left ventricle. After 120 min, the heart was incubated for 5 min at 37°C in a 1% solution of triphenyltetrazolium chloride (TTC). The sizes of the infarcted area and viable ischemic-reperfused area were measured by computed planimetry (Scion Image 1.62; Scion Corporation, Frederick, MD, USA). Infarct size was calculated as described previously (13).

There were no significant differences in the basal hemodynamic parameters, including heart rate, left ventricular pressure, end-diastolic pressure, and positive and negative dP/dt, between WT and KO mice (Table 1). After ischemia, there was no significant difference between the two groups in several parameters such as time to no beating, time to contracture, and left

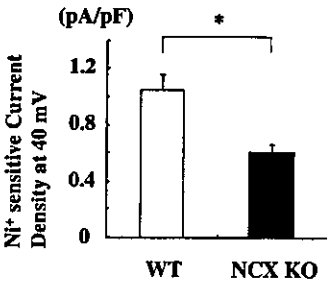

Fig. 1. NCX current densities. The densities of the reverse mode of NCX at 40 mV in ventricular myocytes isolated from WT (n = 9) and NCX KO mice hearts (n = 6). Values are expressed as the mean ± S.E.M. *P<0.05 *vs* WT mice.

Table 1. Hemodynamic parameters of NCX KO mice

	WT (n = 6)	NCX KO (n = 7)
HR (bpm)	356 ± 40	378 ± 77
LVP (mmHg)	142.8 ± 40	146.3 ± 34.5
EDP (mmHg)	4.4 ± 1.5	4.3 ± 1.3
dP/dt (mmHg/s)	7368 ± 630	7845 ± 2582
−dP/dt (mmHg/s)	5204 ± 782	5539 ± 1157
Time to no beating (min)	2.2 ± 0.9	2.2 ± 1.6
Time to contracture (min)	6.2 ± 1.7	6.3 ± 2.0
EDP at 25 min (mmHg)	67.3 ± 9.2	63.8 ± 10.8

HR, heart rate; LVP, left ventricular pressure; EDP, LV end-diastolic pressure; dP/dt and −dP/dt, positive and negative first derivatives for maximal rates of LV pressure development, respectively.

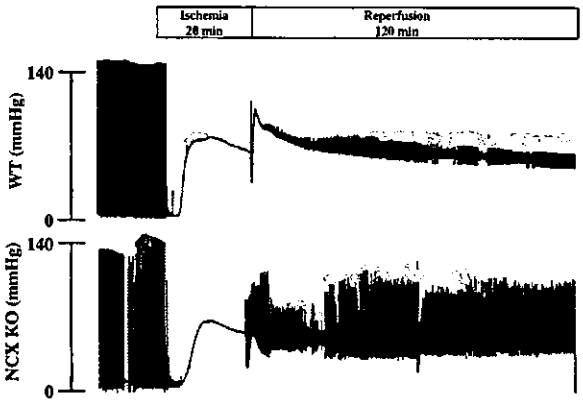

Fig. 2. Ex vivo studies. Changes in LVP during ischemia/reperfusion. Representative LVP records of WT and NCX KO mouse hearts are shown. Note that KO mouse hearts started to contract earlier than WT mouse hearts after reperfusion.

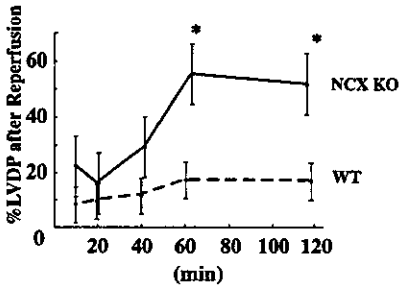

Fig. 3. LVDP of hearts of NCX KO mice (n = 7) and WT mice (n = 6) hearts after reperfusion. Values are expressed as the mean ± S.E.M. **P*<0.05 *vs* WT mice.

ventricular end-diastolic pressure (Fig. 2). After reperfusion, however, hearts of KO mice started to beat earlier than those of WT mice (Fig. 2). At 120 min after reperfusion, contractile function (left ventricular developed pressure) of KO mouse hearts was significantly better (51.7 ± 12.7% of preischemic value) than that of WT mouse hearts (26.3 ± 6.9%, $P<0.05$) (Fig. 3). After ischemia/reperfusion, there was much more viable myocardium in KO hearts than WT hearts (red lesion (printed in black) in Fig. 4A). The infracted size was significantly smaller in KO hearts (32 ± 9%) than in WT hearts (68 ± 10%, $P<0.05$) (white lesion in Fig. 4A and Fig. 4B).

Concluding remarks

Myocardial cell injury is induced by a combination of mechanical and chemical stresses during ischemia

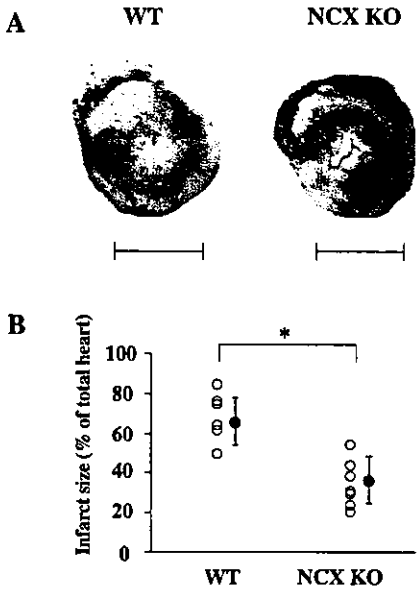

Fig. 4. Infarct size. A: Representative TTC staining photographs of WT and NCX KO mice hearts after ischemia/reperfusion are shown. Infarct area is expressed as a white lesion and viable myocardium is expressed as a red lesion (printed in black). Bar = 2 mm. B: Myocardial infarct size is expressed as percentage for the total heart of WT mice (n = 6) and NCX KO mice (n = 7). Values are expressed as the mean ± S.E.M. **P*<0.05 *vs* WT mice.

(14). Reoxygenation after extended periods of ischemia rapidly induce hypercontracture of cardiomyocytes (15) and aggravate the preexisting injury (16). The hypercontracture represents a major cause of acute lethal cell injury in the reperfused myocardium (17, 18). It has been hypothesized that an increase in intracellular Ca^{2+} levels of cardiomyocytes through NCX induces the hypercontracture state after reperfusion but not during ischemia by the mechanism described below (5). During myocardial ischemia, anaerobic metabolism induces acidosis both inside and outside of cardiomyocytes. The Na^+/H^+ exchanger does not operate at this moment because of no difference in H^+ concentration across the plasma membrane of cardiomyocytes. Reperfusion restores extracellular acidosis, leading to a disparity in H^+ concentration between the inside and outside of cardiomyocytes. The increase in intracellular H^+ concentration activates the Na^+/H^+ exchanger, and the elevated intracellular Na^+ concentration triggers a rise in intracellular Ca^{2+} by the reverse mode of NCX (5). The excessive Ca^{2+} overload induces the catastrophic hypercontracture of cardiomyocytes. In fact, it has been reported that reduction of Ca^{2+} concentration protects cardiomyocytes against hypercontracture evoked by reoxygenation (19). In contrast, overexpression of NCX

increased ischemia/reperfusion injury in mice (20). Pharmacological inhibition of reverse mode of NCX protected reperfusion injury in cardiomyocytes (19). These results suggest that NCX is critically involved in the myocardial ischemia/reperfusion injury; however, NCX inhibitors have been recently reported to be not specific to NCX (6). Two putative NCX inhibitors, KB-R7943 and SEA0400, depressed the Ca^{2+} transients even in cardiomyocytes of NCX null mice (7). Although these NCX inhibitors have been reported to suppress the reverse mode but not the forward mode of NCX, the administration of high dose of these inhibitors increased infarct size possibly by inhibiting the forward mode of NCX (21). We here demonstrated an important role of NCX in myocardial ischemia/reperfusion injury by using NCX KO mice. The reverse mode of NCX current in KO mice was decreased to half that of WT mice. Loss of function of NCX is assumed to result in alleviation of Ca^{2+} overload, hypercontracture, and cell death after reperfusion. Our present study clearly indicates that the inhibition of NCX contributes to cardioprotection against myocardial ischemia/reperfusion injury and suggests that specific inhibitors of the reverse mode of NCX may be useful to prevent the myocardial ischemia/reperfusion inury.

Acknowledgments

We thank to Y. Reien for the current density analysis and R. Kobayashi, E. Fujita, M. Watanabe, M. Iida, and A. Ohkubo for technical assistance. This work was supported in part by grants from the Japanese Ministry of Education, Culture, Sports, Science, and Technology and the Japan Health Sciences Foundation.

References

1 Schulze D, Kofuji P, Hadley R, Kirby MS, Kieval RS, Doering A, et al. Sodium/calcium exchanger in heart muscle: molecular biology, cellular function, and its special role in excitation-contraction coupling. Cardiovasc Res. 1993;27:1726–1734.

2 Bridge JH, Smolley JR, Spitzer KW. The relationship between charge movements associated with I_{Ca} and $I_{Na\text{-}Ca}$ in cardiac myocytes. Science. 1990;248:376–378.

3 Kleber AG. Resting membrane potential, extracellular potassium activity, and intracellular sodium activity during acute global ischemia in isolated perfused guinea pig hearts. Circ Res. 1983; 52:442–450.

4 Pilitsis JG, Diaz FG, O'Regan MH, Phillis JW. Inhibition of Na^+/Ca^{2+} exchange by KB-R7943, a novel selective antagonist, attenuates phosphoethanolamine and free fatty acid efflux in rat cerebral cortex during ischemia-reperfusion injury. Brain Res. 2001;916:192–198.

5 Eigel BN, Hadley RW. Antisense inhibition of Na^+/Ca^{2+} exchange during anoxia/reoxygenation in ventricular myocytes. Am J Physiol Heart Circ Physiol. 2001;281:H2184–H2190.

6 Reuter H, Henderson SA, Han T, Matsuda T, Baba A, Ross RS, et al. Knockout mice for pharmacological screening: testing the specificity of Na^+/Ca^{2+} exchange inhibitors. Circ Res. 2002; 91:90–92.

7 Wakimoto K, Kobayashi K, Kuro OM, Yao A, Iwamoto T, Yanaka N, et al. Targeted disruption of Na^+/Ca^{2+} exchanger gene leads to cardiomyocyte apoptosis and defects in heartbeat. J Biol Chem. 2000;275:36991–36998.

8 Suzuki M, Li RA, Miki T, Uemura H, Sakamoto N, Ohmoto-Sekine Y, et al. Functional roles of cardiac and vascular ATP-sensitive potassium channels clarified by Kir 6.2-knockout mice. Circ Res. 2001;88:570–577.

9 Watanabe Y, Kimura J. Inhibitory effect of amiodarone on Na^+/Ca^{2+} exchange current in guinea-pig cardiac myocytes. Br J Pharmacol. 2000;131:80–84.

10 Kimura J, Miyamae S, Noma A. Identification of sodium-calcium exchange current in single ventricular cells of guinea-pig. J Physiol (Lond). 1987;384:199–222.

11 Zou Y, Komuro I, Yamazaki T, Kudoh S, Uozumi H, Kadowaki T, et al. Both Gs and Gi proteins are critically involved in isoproterenolinduced cardiomyocyte hypertrophy. J Biol Chem. 1999;274:9760–9770.

12 Takimoto E, Yao A, Toko H, Takano H, Shimoyama M, Sonoda M, et al. Sodium calcium exchanger plays a key role in alteration of cardiac function in response to pressure overload. FASEB J. 2002;16:373–378.

13 Suzuki M, Sasaki N, Miki T, Sakamoto N, Ohmoto-Sekine Y, Tamagawa M, et al. Role of sarcolemmal K(ATP) channels in cardioprotection against ischemia/reperfusion injury in mice. J Clin Invest. 2002;109:509–516.

14 Piper HM, Garcia-Dorland D, Ovize M. A fresh look at reperfusion injury. Cardiovasc Res. 1998;38:291–300.

15 Siegmund B, Koop A, Klietz T, Schwartz P, Piper HM. Sarcolemmal integrity and metabolic competence of cardiomyocytes under anoxiareoxygenation. Am J Physiol. 1990;258: H285–H291.

16 Stern MD, Chien AM, Capogrossi MC, Pelto DJ, Lakatta EG. Direct observation of the "oxygen paradox" in single rat ventricular myocytes. Circ Res. 1985;56:899–903.

17 Barrabes JA, Garcia-Dorado D, Ruiz-Meana M, Piper HM, Solares J, Gonzalez MA, et al. Myocardial segment shrinkage during coronary reperfusion in situ. Relation to hypercontracture and myocardial necrosis. Pflugers Arch. 1996;431:519–526.

18 Ganote CE. Contraction band necrosis and irreversible myocardial injury. J Mol Cell Cardiol. 1983;15:67–73.

19 Schafer C, Ladilov Y, Inserte J, Schafer M, Haffner S, Garcia-Dorado D, et al. Role of the reverse mode of the Na^+/Ca^{2+} exchanger in reoxygenation-induced cardiomyocyte injury. Cardiovasc Res. 2001;51:241–250.

20 Cross HR, Lu L, Steenbergen C, Philipson KD, Murphy E. Overexpression of the cardiac Na^+/Ca^{2+} exchanger increases susceptibility to ischemia/reperfusion injury in male, but not female, transgenic mice. Circ Res. 1998;83:1215–1223.

21 Inserte J, Garcia-Dorado D, Ruiz-Meana M, Padilla F, Barrabes J, Pina P, et al. Effect of inhibition of Na^+/Ca^{2+} exchanger at the time of myocardial reperfusion on hypercontracture and cell death. Cardiovasc Res. 2002;55:739.